Journal of Geosciences and Geomatics, 2017, Vol. 5, No. 6, 267-283
Available online at http://pubs.sciepub.com/jgg/5/6/2

DOI:10.12691/jgg-5-6-2

New LA-ICP-MS U-Pb Ages, Lu-Hf Systematics and REE Characterization of Zircons from a Granitic Pluton in the Betare Oya Gold District, SE Cameroon

Kevin I. Ateh[1,*], Cheo E. Suh[1,4], Elisha M. Shemang[2], A. Vishiti[3,4], Enerst Tata[1], Nelson N. Chombong[1]

[1]Economic Geology Unit, Department of Geology, University of Buea, P.O. Box 63 Buea, South West Region, Cameroon
[2]Department of Earth and Environmental Sciences, Botswana International University of Science and Technology, Private Bag 16, Palapye, Botswana
[3]Higher Institute of Science, Engineering and Technology, Cameroon Christian University Institute, P.O. Box 5, Bali, North West
[4]Department of Geology, Mining and Environmental Science, University of Bamenda, P.O. Box 39, Bamenda, North-West Region, Cameroon
*Corresponding author: kevinateh@gmail.com

Abstract A combination of whole rock geochemistry, Ti-in-zircon thermometry, geochronology and Lu-Hf isotope composition of zircon is employed in this study to depict the source of a granitoid from the Bétaré Oya Gold District, its formation temperature, age of emplacement and evaluate the role of petrogenesis and magmatic evolution of the granitic melt in hydrothermal fluid circulation and primary gold precipitation. In this contribution, zircon grains from a granitic pluton were analyzed for their internal structures using cathodoluminescence imagery and dated by U-Pb technique using LA-ICP-MS. Based on the zircon internal structure, magmatic and metamorphic zircons are distinguished. The granitoid reveal a mean age of 635 Ma similar to those obtained from granitic intrusions along the Central African Shear Zone (CASZ) in Cameroon. This age defines a narrow Pan African emplacement age for the pluton and a unique melting event synchronous with magmatism and deformation. It also depicts a new and older mineralization along the CCSZ at 620-635 Ma for the Bétaré Oya Gold District, SE Cameroon. Ti-in-zircon thermometry indicates their emplacement at a modal temperature range between 625°C and 775°C. Based on whole rock geochemistry alongside trace and REE composition of zircon, the pluton shows a granodioritic to tonalitic affinity. The granitoid is sub alkaline with a high K calc-alkaline affinity, peraluminous and of I-type. REE in zircon patterns display high Ce concentrations, negative Eu anomalies, HREE enrichment, $^{176}Lu/^{177}Hf$ ratio < 0.022 and negative ε_{Hf} values that range from -5.29 to -0.12. Positive ε_{Hf} values suggest a mafic crustal contribution. Across the Atlantic into NE Brazil, mineralization is often associated to late Pan African event. We disclose an early mineralization event at 635-620Ma in the region.

Keywords: *Granitoid, geochemistry, Ti-in-zircon thermometry, zircon chemistry, geochronology*

Cite This Article: Kevin I. Ateh, Cheo E. Suh, Elisha M. Shemang, A. Vishiti, Enerst Tata, and Nelson N. Chombong, "New LA-ICP-MS U-Pb Ages, Lu-Hf Systematics and REE Characterization of Zircons from a Granitic Pluton in the Betare Oya Gold District, SE Cameroon." *Journal of Geosciences and Geomatics*, vol. 5, no. 6 (2017): 267-283. doi: 10.12691/jgg-5-6-2.

1. Introduction

Several hydrothermal ore deposits are formed within and at some distance from felsic to intermediate igneous intrusions although a direct genetic link with these intrusions is not always clear [1]. It is therefore necessary to constraint the ages and petrogenesis of plutons within metallogenic belts to allow for comparison of such felsic bodies with other intrusions associated with ore deposits worldwide. Skarn deposits in NE Brazil have often been related to granitic intrusions within a meta-sedimentary sequence (marble, quartzite and schist) characterized by late Braziliano-Pan African mineralization (W, Au, Mo, Pb-Zn, Sn). However across the Atlantic into the central African region the mineralization - granitoid relationship still remains obscure. Zircon is a stable mineral that can crystallize over a wide range of magmatic temperatures, essentially depending on the bulk composition of the host magma [2] and could be sourced from different rock types with different elemental compositions. The composition of zircon (trace/REE, HFSE, U, Th concentrations) and the shape and slope of chondrite-normalized patterns bear characteristic features of zircon grains of a particular magmatic system [3]. The chemical composition of zircon is used to determine various magmatic processes such as fractional crystallization, interaction with hydrothermal fluids and/or magma mixing [4]. The ability for zircon to incorporate trace and rare earth elements such as U, Pb and Hf in its crystal structure makes it ideal for geochemistry, geochronology and isotopic studies.

According to [5], Lu-Hf systematics on zircon grains is of great significance when combined with the U-Pb method as it gives the possibility to characterize isotopically the host magma from which they crystallized and unravel the history of crustal growth. Cathodoluminesence Back Scattered Electron (CL-BSE) images of zircon grains reveal its chemical zonation and the internal growth structure essential in understanding the evolution of the magmatic system.

The eastern region of Cameroon is the most prospective area for gold in the country (Figure 1). This gold district extends beyond its borders into the Central African Republic. Research in this region has focused on understanding the style of mineralization [6]. Previous studies in the area also highlight the significance of granitic plutons in the genesis of gold mineralization [7,8]. According to [7] granitoids from the Batouri Gold District varies in age from 619 ± 2 Ma to 624 ± 2 Ma, are high K calc-alkaline and related to gold mineralization. The ages of granitoids related to mineralization in the Bétaré Oya Gold District are not known. This area is known for its alluvial gold mining. This paper therefore focuses on a granitic body from the Bétaré Oya area (Figure 1), one of several plutonic bodies along the Central Cameroon Shear Zone (CCSZ). The aureole of this pluton is gold-bearing and characterized by sheared lithologies. Recently obtained combined aeromagnetic and radiometric data (Figure 1a) from this area indicates the pluton as the most prominent feature. We therefore use zircon chemistry alongside Lu-Hf isotope data of zircon grains to depict the source, constraint the age of the granitoid emplacement and evaluate the role of petrogenesis and magmatic evolution of the granitic melt in hydrothermal fluid circulation and primary gold precipitation in the Bétaré Oya area. We further compare this to mineralized intrusive bodies along the CCSZ and around the world. Generally, aureoles around felsic igneous intrusions present prospective areas for mineral exploration. In this area the aureole around this plutonic body is currently being exploited for gold through artisanal and semi mechanized mining methods (Figure 1c).

2. Regional Geology

The Central Cameroon Shear Zone (CCSZ) is the SW extension of the Central African Shear Zone (CASZ) and constitutes a part of the Central African Fold Belt (CAFB). It is situated at the northern edge of the Congo Craton [9] and composed largely of Palaeoproterozoic basement, which can be traced through Cameroon across the Atlantic into northeastern Brazil and the Trans-Sahara Belt [10]. In Pre-drift reconstruction of West Gondwana, the Pan-African/Braziliano belts of Cameroon, Nigeria and the Borborema province are sandwiched between the Congo-Saõ Francisco and West African Cratons hence occupy a strategic position in unraveling the geodynamic evolution of these regions [11,12]. The CCSZ and its relay feature known as the Sanaga faults (SF) have a NE-SW orientation and is characterized by the abundance of granitic intrusions associated with major shear zones [7,13,14]. Although Pan-African granites constitute a common lithology in the country, their origin remains poorly understood. Intrusive bodies along the CCSZ are generally Pan-African (560 - 686 Ma) in age [7,15,16,17,18]. However, an earlier Tonien - Stenien overprint event at 911 to 1127 Ma [7] have been reported in the Batouri area indicating an extended unique melting event contemporaneous with the magmatism responsible for the emplacement of granitoid in the other domains of the CCSZ. The Lom basin is a syn-depositional Neoproterozoic pull apart basin [19]. It is sandwiched by strike slip faults known as the Sanaga Fault (SF) a relay of the CCSZ system [19,20]. The SF is a continental scale transcurrent fault. It is a potentially deep tapping crustal fault that has focused gold-bearing fluids into structures in the Lom Basin [21]. The Lom basin is composed mainly of meta-sedimentary rocks, grouped into two main structural and metamorphic units. These units include a monocyclic unit which is composed of volcano-clastic series, orthogneiss, quartzite and polygenic conglomerate [22] metamorphosed under green schist facies and associated with grabens. The polycyclic unit consists of staurolite micaschists, Lom bridge gneisses, and staurolite-chloritoid mylonites, closely related to the horst structures [19]. The mylonites are the main identifying features for the presence of the SF [22]. These units are intruded by quartz veins and granitoids (granite, monzonite and lamprophres) which show evidence of sinistral deformation. This region is known for its gold mineralization hosted within quartz veins [6]. The quartz veins are associated with schist and believed to be products of hydrothermal fluids which originated from nearby intrusive bodies. They generally have a N70°E foliation conformable to the CCSZ shear zone system.

3. Samples/Analytical Techniques

Three samples were collected from the study area; two (02) granitic rock chips and a pack (01) of granitic saprolite weighing about 5 kg (see Figure 1d). The granitoid is coarse-grained and displays a porphyritic texture with quartz and plagioclase mega phenocrysts set in a mica-quartz dominated groundmass. Mineralogically, the granitoid is composed of quartz (50-65%), K-feldspars (15-25%), biotite (15-20%) and hornblende (<5%). Accessory minerals present include: apatite, titanite, spene, zircons, secondary carbonates and opaque minerals. Plagioclase occurs as subhedral to anhedral crystals with variable inclusions of zircon, apatite, and biotite. Quartz occurs as closely packed grains and elongate ribbons that display undulatory extinction. K-feldspar occurs as fine to medium anhedral crystals interstitial to plagioclase and quartz and includes microperthitic microcline and orthoclase. Biotite occurs as pleochroic green to reddish brown flakes partly altered to chlorite. Hornblende occurs as large, subhedral prismatic crystals which are altered to chlorite in some places. Titanite occurs as fine to medium-grained idiomorphic crystals interstitial to plagioclase, hornblende, biotite, and quartz. These samples were shipped to the University of California, Santa Barbara, USA for zircon chemistry, geochronology and Lu-Hf isotope analyses.

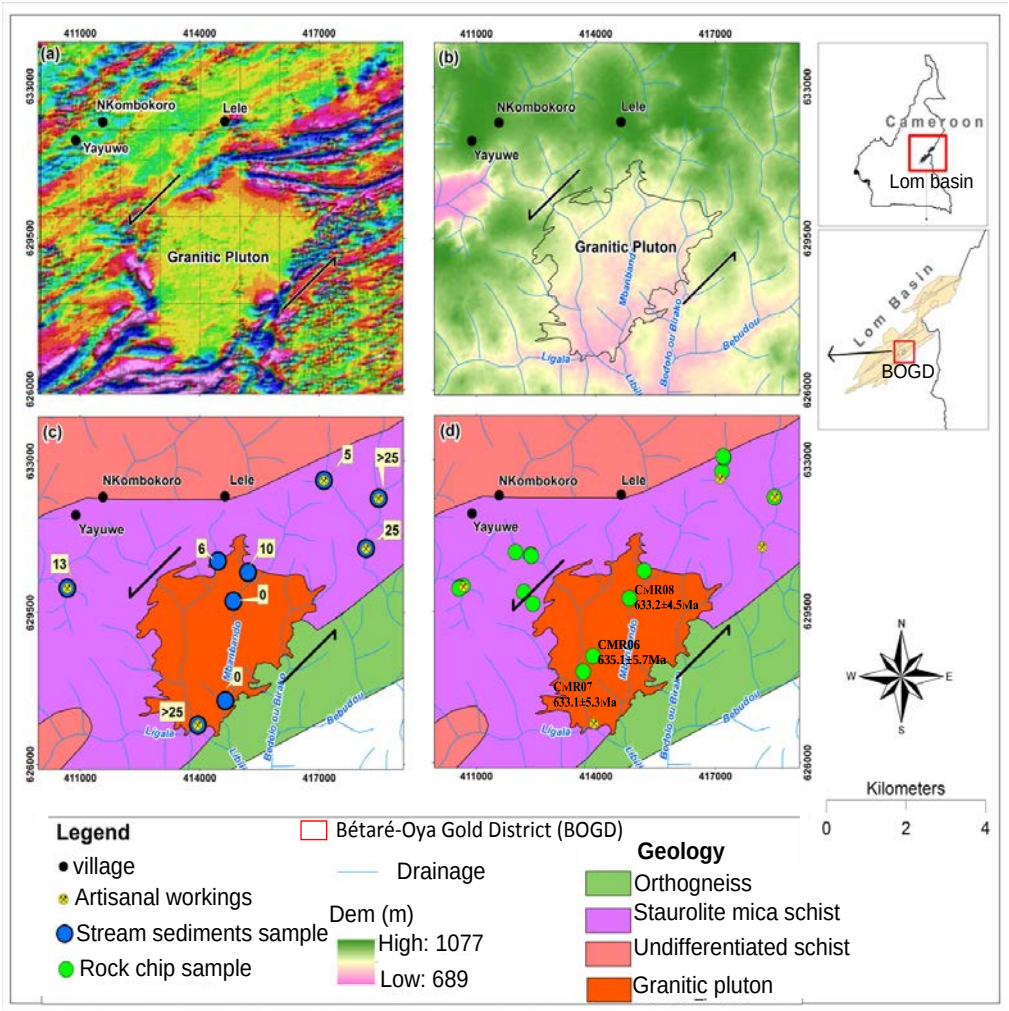

Figure 1. a - Aeromagnetic and radiometric image of the Bétaré-Oya Gold District-BOGD, Lom basin, eastern Cameroon **b** - Elevation and drainage map of the study area **c** - Stream sediment sample location map with gold count per location (gold particles per 10 kg pan) in proximity to artisanal mining sites **d** - Rock sample location map with ages of dated samples displayed

3.1. Sample Preparation

The granitoid samples were crushed and zircons separated by standard techniques (Rogers's water table, Frantz magnetic separation, and methylene iodide heavy-liquid separation) at the Department of Earth Science, University of California Santa Barbara, USA (UCSB). Zircons were mounted in separate epoxy plugs, ground down to expose grain interiors and polished with 6 µm and 1 µm diamond paste Prior to analytical work, zircons were examined for zoning using a cathodoluminescence (CL) system attached to a FEI Quanta400f Scanning Electron Microscope house at UCSB.

3.2. Zircon U-Pb and Trace Element Analyses

U-Th/Pb isotope and trace element concentration data were collected using a split stream inductively coupled plasma mass spectrometry (LASS-ICPMS) facility located at UCSB. Methods follow those outlined in [23] with modifications as presented in [24] and are briefly summarized here. Instrumentation consists of a Photon Machines 4-ns pulse duration 193-nm wavelength ArF excimer laser attached to a Nu Plasma HR multi-collector (MC) ICPMS set to measure U, Th, and Pb isotope ratios and an Agilent 7700S Quadruple ICPMS to measure trace element concentrations. Analytical conditions of the laser for zircon were a 25µm spot, 4Hz frequency, a laser energy of 100% of 3mJ (equating to a fluence of ~1.7 J/cm^2) and 100 shots per analysis.

U-Th/Pb data reduction, including corrections for baseline, instrumental drift, mass bias, down-hole fractionation and uncorrected age calculations were carried out using Igor Pro and the plugin Iolite v. 2.5 (see [25] for details on data reduction methodology). Primary reference zircon "91500" [1065 Ma $^{206}Pb/^{238}U$ isotope dilution-thermal ionization mass spectrometry age, [26]] was used to monitor and correct for instrumental drift, mass bias, and down-hole inter-element fractionation. To monitor data accuracy, secondary reference zircon "GJ1" (601.7 ± 1.3 Ma, [27]) was analyzed concurrently (once every 8 unknowns) and mass bias- and fractionation-corrected based on measured isotopic ratios of the primary reference material. During the analytical period, repeat analyses of GJ-1 gave a weighted mean $^{206}Pb/^{238}U$ age of 599 ± 1 Ma, mean square weighted deviation (MSWD) = 0.8, $^{207}Pb/^{206}Pb$ age of 601 ± 3 Ma, MSWD = 0.8, n = 70. Zircon trace element concentrations were normalized to zircon GJ-1 (using the reference values of [28]), using ^{90}Zr as an internal standard and, based on the long-term reproducibility of multiple secondary reference zircons, are accurate to 3-5%. All uncertainties are quoted at 2σ

and include contributions from the reproducibility of the reference materials for $^{207}Pb/^{206}Pb$, $^{206}Pb/^{238}U$ and $^{207}Pb/^{235}U$. U-Th/Pb data were plotted using the Redux v.3.0.4 [29]. The complete U-Th/Pb and trace element data are presented in Table 1 and Table 2.

3.3. Zircon Lu-Hf Isotope Analyses

The same zircon domains that had been analyzed for U-Pb were analyzed for their Lu-Hf isotopic composition at UCSB, following the method described in [23,30]. Data were collected on a Nu Plasma MC-ICPMS using a spot size of 40µm, laser energy of 3 mJ, at 10Hz, and 500 shots. Whenever possible the Lu-Hf laser spot was drilled directly on top of the LASS laser spot. Replicate measurements yield $^{176}Hf/^{177}Hf$ values of 0.282506 ± 0.00002 (2σ, n=25), 0.282473 ± 0.00007 (n=7), 0.282323 ± 0.00007 (n=5), and 0.282128 ± 0.00003 (n=7) for reference zircons Mud Tank, Plesovice, 91500, and synthetic zircon "MUN3" respectively. For calculation of εHft values the decay constant of 1.867 × 10−11 (average of [31] and [32]) and the values for the chondritic uniform reservoir (CHUR, ^{176} Lu/ ^{177}Hf = 0.0336, ^{176} Hf/ ^{177} Hf = 0.282785; [33]) were used. The initial $^{176}Hf/^{177}Hf$ ratios and εHft for all analyzed zircon domains were calculated for the corresponding ^{206} Pb/ ^{238}U age of the sample. A two stage depleted mantle Hf model age (TDM, in Ga) was calculated from the initial ^{176}Hf/ ^{177}Hf of each zircon at the time of crystallization (in terms of the apparent $^{206}Pb/^{238}U$ age) by using ^{176} Hf/ ^{177}Hf = 0.28325 and ^{176} Lu/^{177} Hf = 0.0384 for the bulk earth [33] and ^{176} Lu/ 177 Hf = 0.0113 for the average crust. Ti-in zircon temperature calculated as outline in [34].

4. Results

4.1. Whole Rock Geochemistry

The whole rock geochemical data for the studied granitoid samples alongside the Batouri granitoid [7] and the two mica granite [16] from Ekomédion are represented in Table 1. Samples CMR06, CMR07 and CMR08 show a similar compositional range for SiO_2 (67.52, 66.42 and 65.38), Al_2O_3 (15.89, 16.25, and 16.6), Fe_2O_3 (3.5, 3.66 and 3.87) Na_2O (3.81, 3.98 and 4.21) K_2O (3.66, 3.33 and 2.73) and CaO (2.72, 0.23 and 3.74) respectively. According to the classification scheme of [35,36,37], the Bétaré Oya granitoid is sub-alkaline with a high-K calc-alkaline affinity (Figure 2a, Figure 2b). On the A/NK versus A/CNK classification plot [38], the granitoid is granodioritic to tonalitic in composition. They are peraluminous with all samples clustering within the 'I-type' field (Figure 2c). Nb - Y discrimination plot [39], reveals a volcanic arc setting for that the Bétaré Oya granitoid (Figure 2d).

Table 1. Major oxides and trace element composition for the Bétaré-Oya (this study), Batouri [7] and Ekomédion [16] granitoids

XRF-wt%	Bétaré Oya			Batouri											Ekomédion		
	CMR7A	CMR7B	CMR8	L44	L45	L46	L57	L59	L21	L41m	L42	L43	L54	L56	EK24	EK25	EK28
SiO_2	67.5	66.4	65.4	72.6	71.1	72.1	72.0	73.4	66.8	65.6	65.8	65.4	66.4	67.5	73.7	73.3	73.5
TiO_2	0.7	0.7	0.8	0.3	0.4	0.4	0.3	0.3	0.6	0.7	0.8	0.8	0.7	0.6	0.2	0.2	0.2
Al_2O_3	15.9	16.3	16.6	14.3	14.3	14.0	14.2	13.6	15.3	15.4	15.6	16.5	16.2	16.0	14.1	14.0	13.8
Fe_2O_3	3.5	3.7	3.9	2.1	2.9	2.9	2.5	2.3	3.9	5.9	4.3	3.9	3.7	3.4	1.6	1.6	0.6
MnO	0.0	0.1	0.0	0.0	0.0	0.1	0.0	0.1	0.1	0.1	0.1	0.1	0.1	0.0	0.0	0.0	<.01
MgO	1.1	1.3	1.5	0.3	1.0	0.7	0.3	0.3	1.6	1.4	2.0	1.5	1.3	1.1	0.3	0.3	0.1
CaO	2.7	3.2	3.7	1.2	1.8	1.5	1.3	1.2	3.4	3.2	3.6	3.7	3.2	2.7	0.9	0.9	0.9
Na_2O	3.8	4.0	4.2	3.4	2.5	3.8	3.5	3.3	3.5	4.0	3.6	4.1	4.0	3.8	2.8	2.9	3.0
K_2O	3.7	3.3	2.7	5.2	4.8	3.5	5.2	5.1	3.7	2.7	3.2	2.7	3.3	3.6	5.6	5.4	5.3
P_2O5	0.3	0.2	0.3	0.1	0.1	0.1	0.1	0.1	0.2	0.2	0.2	0.3	0.2	0.2	0.1	0.1	0.1
LOI	0.4	0.4	0.7	0.4	0.5	0.6	0.4	0.3	0.5	0.5	0.6	0.6	0.4	0.5	0.7	0.5	0.5
Total	**99.6**	**99.6**	**99.8**	**99.8**	**99.6**	**99.8**	**99.7**	**99.8**	**99.6**	**99.7**	**99.7**	**99.6**	**99.5**	**99.5**	**99.8**	**99.1**	**97.9**
ppm																	
Rb	85	114	108	141	121	140	134	142	91	104	113	83	68	78	379	407	361
Ba	1477	936	679	607	1816	708	843	753	1113	676	936	1472	1847	1863	455	445	418
Th	5	10	8	22	30	14	18	19	8	17	8	5	11	12	60	59	46
U	bdl	bdl	bdl	bdl	bdl	bdl	bdl	bdl	bdl	bdl	bdl	bdl	bdl	bdl	9.0	8.8	11.6
Nb	10	10	10	10	9	13	10	10	10	8	10	8	8	8	31.9	31.8	31.8
La	bdl	27.9	52.8	57.6	44.1	30.5	bdl	bdl	17.3	53.7	28.2	bdl	42	52	86	73.3	55.8
Ce	bdl	47	79	99	77	59	bdl	bdl	44	88	49	bdl	72	91	156	133	105
Sr	714	525	404	106	370	182	108	100	480	403	523	707	688	570	127	116	110
Nd	33	33	64	45	56	36	79	64	46	63	35	31	57	51	57	50	40
Zr	232	199	294	238	448	161	280	269	161	295	198	229	254	229	176.3	170.8	134.3
Hf	bdl	5	4	5	8	5	bdl	bdl	4	3	4	bdl	4	5	5.81	5.71	4.5
Sm	bdl	5.8	6.1	5.8	4.4	3.5	bdl	bdl	4	5.5	3.9	bdl	4.2	3.6	9.82	8.89	7.3
Eu	bdl	2.1	bdl	0.7	1.4	0.8	bdl	bdl	1.2	bdl	1	bdl	1.2	1.5	0.82	0.68	0.62
Y	12	19	26	28	17	21	31	43	22	24	16	13	13	9	19.5	19	20.8
Yb	bdl	1.4	1.5	2.8	1.8	2.7	bdl	bdl	2.4	1.2	1.5	bdl	0.9	0.8	1.86	1.89	2.07
Lu	bdl	0.22	0.19	0.46	0.28	0.5	bdl	bdl	0.37	0.18	0.23	bdl	0.17	0.17	0.24	0.26	0.3
V	55	72	84	10	44	26	8	7	67	86	70	59	54	37	18.4	18	15.9
Ta	bdl	bdl	bdl	2.9	bdl	bdl	bdl	bdl	bdl	bdl	bdl	bdl	bdl	bdl	3.14	3.23	3.5
Rb/Sr	0.12	0.22	0.27	1.33	0.33	0.77	NA	NA	0.19	0.26	0.22	bdl	0.10	0.14	2.99	3.53	3.29
Rb/Ba	0.06	0.12	0.16	0.23	0.07	0.20	NA	NA	0.08	0.15	0.12	bdl	0.04	0.04	0.83	0.92	0.86
Zr/Hf	NA	39.8	73.5	47.6	56.0	32.2	NA	NA	40.3	98.3	49.5	NA	63.5	45.8	30.3	29.9	29.8
Na+K	7.47	7.31	6.94	8.54	7.33	7.34	8.62	8.37	7.15	6.67	6.76	6.81	7.31	7.44	8.38	8.29	8.27
A/CNK	1.08	1.07	1.09	1.07	1.14	1.10	1.03	1.04	0.97	1.01	0.98	1.00	1.02	1.06	1.02	1.02	1.02
A/NK	1.43	1.51	1.63	1.28	1.53	1.39	1.25	1.24	1.58	1.63	1.67	1.71	1.60	1.57	1.11	1.12	1.11

*NA: Not Applicable; bdl: below detection limit. Na+K= $Na_2O + K_2O$; A/CNK = molar Al_2O_3/ CaO + $Na_2O + K_2O$; molar A/NK = $Al_2O_3/Na_2O + K_2O$

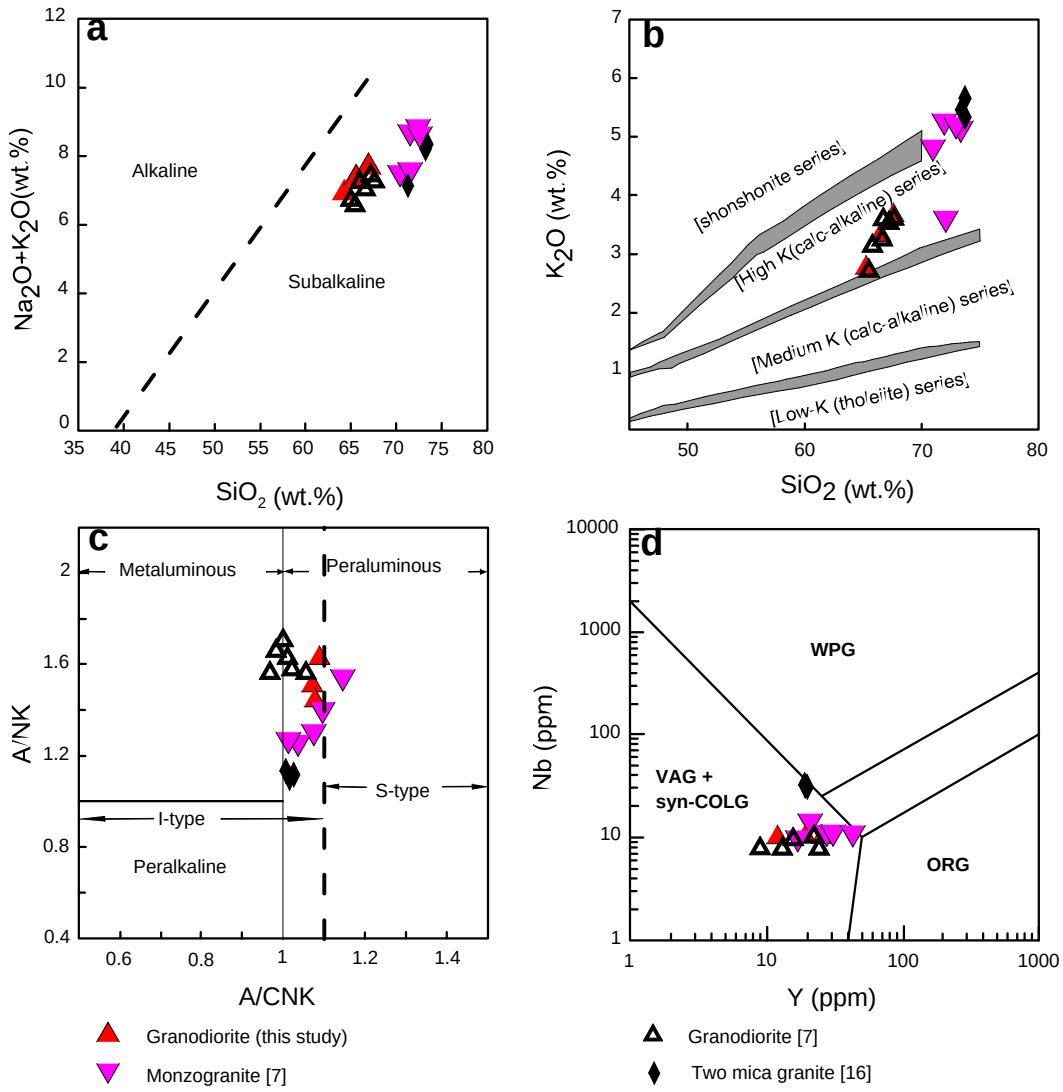

Figure 2. Major element geochemical classification plots for granitoid rocks from Bétaré Oya. (a) $Na_2O + K_2O$ versus SiO_2 diagram of [35], showing the subalkaline compositions of the rocks. (b) K_2O versus SiO_2 diagram of [37], the rocks plot in the high-K field. (c) A/NK versus A/CNK diagram of [38] showing aluminosity and alkalinity. (d) Discrimination diagram of [39], showing that the rocks were formed in a volcanic arc setting. A/NK = molar Al_2O_3/Na_2O+K_2O; A/CNK= molar $Al_2O_3/CaO+Na_2O+K_2O$, Syn-COLG, Syn-collisional granitoid; WPG, within-plate granitoid; VAG, volcanic arc granitoid; ORG, oceanic ridge granitoid

4.2. Zircon Morphology and Composition

Representative CL images of zircon grains from the investigated granitic pluton are provided in Figure 3. Based on their internal structures five (05) different zircon populations have been identified: (i) Zircon grains with consistent oscillation zoning from core to rim, equant to elongated grains (Figure 3, 07Z05). The variation of CL intensity results in a light/dark zone alternation (06Z25). (ii) Zircon grains that are euhedral to subhedral with light and /or distorted core and a clear zoning towards the darker rim (Figure 3, 07Z20, 07Z24 and 08Z10). In some grains the core is zoned (Figure 3, 07Z19). (iii) Subhedral to euhedral grains characterized by relatively small, thin and elongated dark cores with thick light mantles and a thin dark rim (Figure 3, 07Z29). The dark core in some grains is clearly absent (Figure 3, 08Z06) whereas in others the dark core is thick and constitutes a thin light mantle (iv) Sub rounded crystals (Figure 3 (06Z24, 08Z26) with thick light core and an apparent zoning in some cases and a thin dark rim. (v) Distorted zircon grains some of which portray irregular to no zoning at all (Figure 3, 07Z07) and the others with a distorted core but zoned rims (06Z04). The boundary between the distorted core and zoned rim in some grains is marked by thin light band (07Z24, Figure 3). In this study Ti concentration in the zircon grains ranges from ~1 ppm to 330 ppm with approximately 83% of the analyzed grains with values ≤ 20 ppm (Table 2). Crystallization temperature for each grain varies from ~ 560°C to 1230°C with modal temperatures of 700±2°C Figure 4 (a to d). The concentrations of Rare Earth Elements (REE) vary greatly from La - Lu. Ce values in sample CMR06 range between 0.74 - 264 ppm, CMR07 between 1.33-1660 ppm and CMR08 between 4.14-1560 ppm. These values are generally higher than those of neighboring Pr, with all La values below the detection limits. Pr values range between 0.3-32.9 ppm in CMR06, 0.112-149 ppm in CMR07 and 0.52-367 ppm in CMR08. Eu values are generally depleted relative to Sm and Gd. Figure 5 (a, b and c) show REE patterns for CMR06, CMR07 and CMR08 respectively. These patterns generally portray high Ce values, negative Eu anomalies and HREE enrichment. However sample CMR08 shows a dual character of

depletion and enrichment in Eu (Figure 5c). On Zircon/chondrite normalized patterns, REE of zircon grains from the three (03) samples investigated revealed three (03) patterns: (i) one with high concentrations in Ce accompanied by a negative Eu anomaly and HREE enrichment, (ii) high Ce concentrations, positive Eu anomaly and HREE enrichment and (iii) progressive enrichment from LREE to HREE.

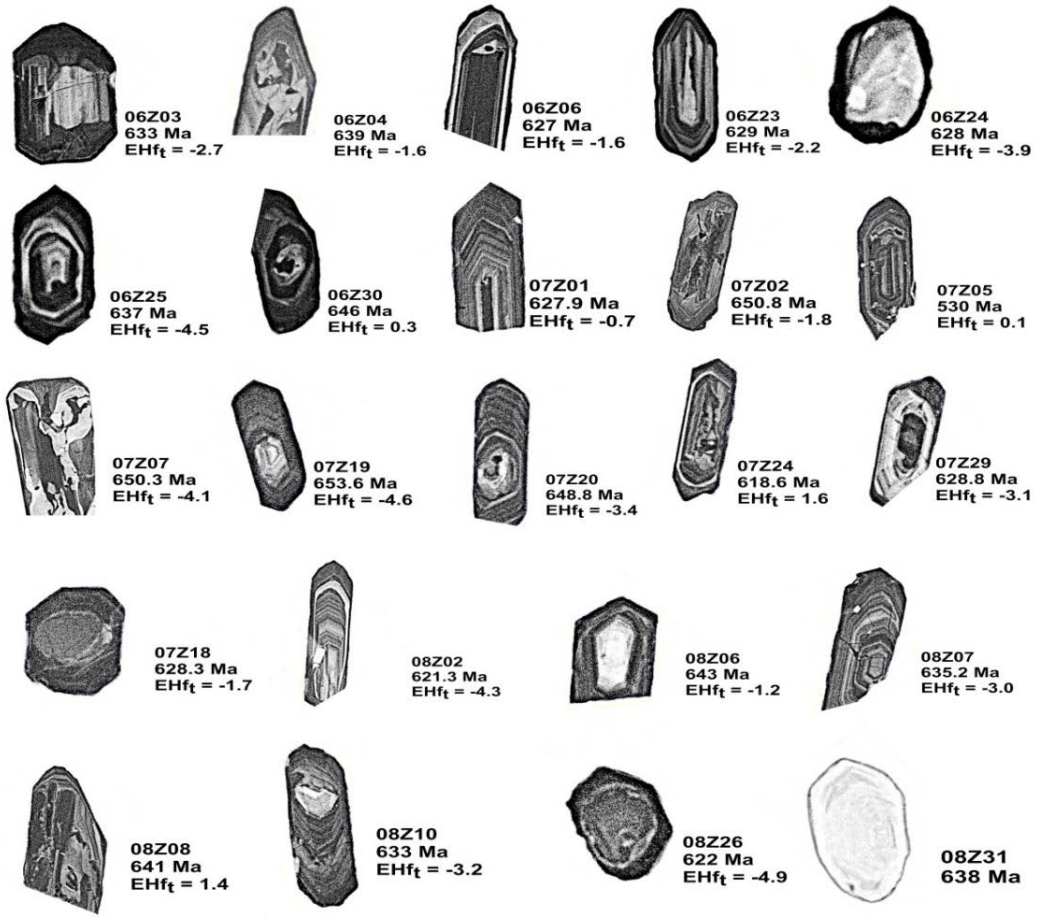

Figure 3. CL images of zircon crystals analyzed from the Bétaré Oya granitic pluton

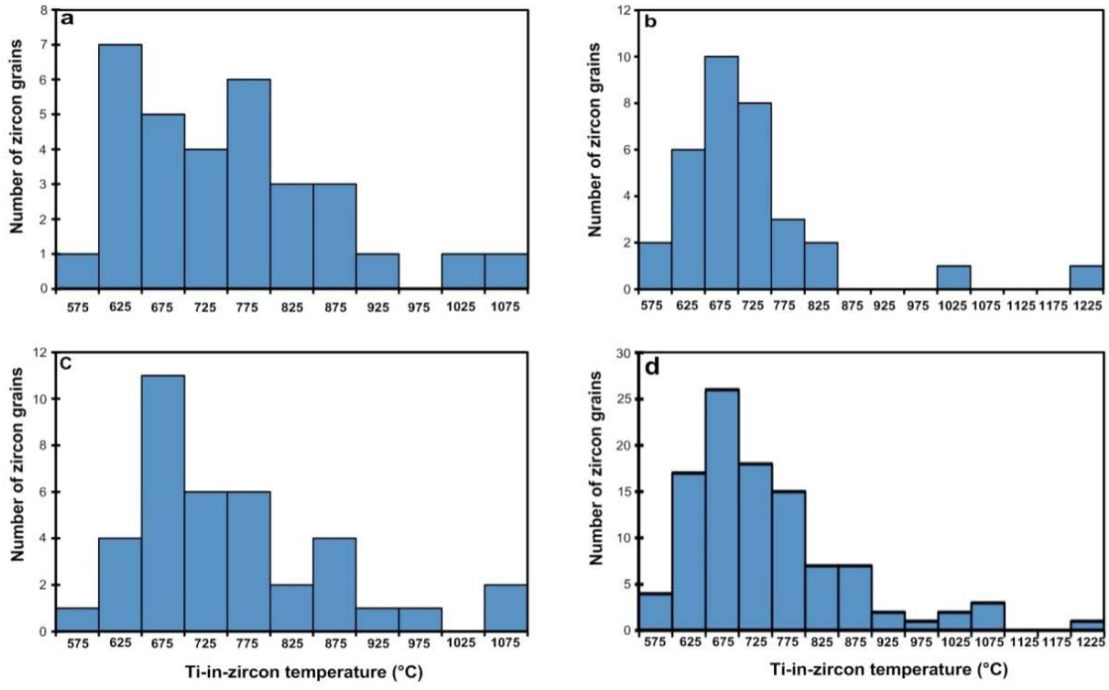

Figure 4. Zircon crystallization temperature of the various granitic samples obtained through Ti-in-zircon thermometry[34]. a - Temperature variation in zircon grains from sample CMR06. b - Temperature variation in zircon grains from sample CMR07 c - Temperature variation in zircon grains from sample CMR08. d - Temperature variation in all three samples combined. The mean temperature is 700 ± 2 °C

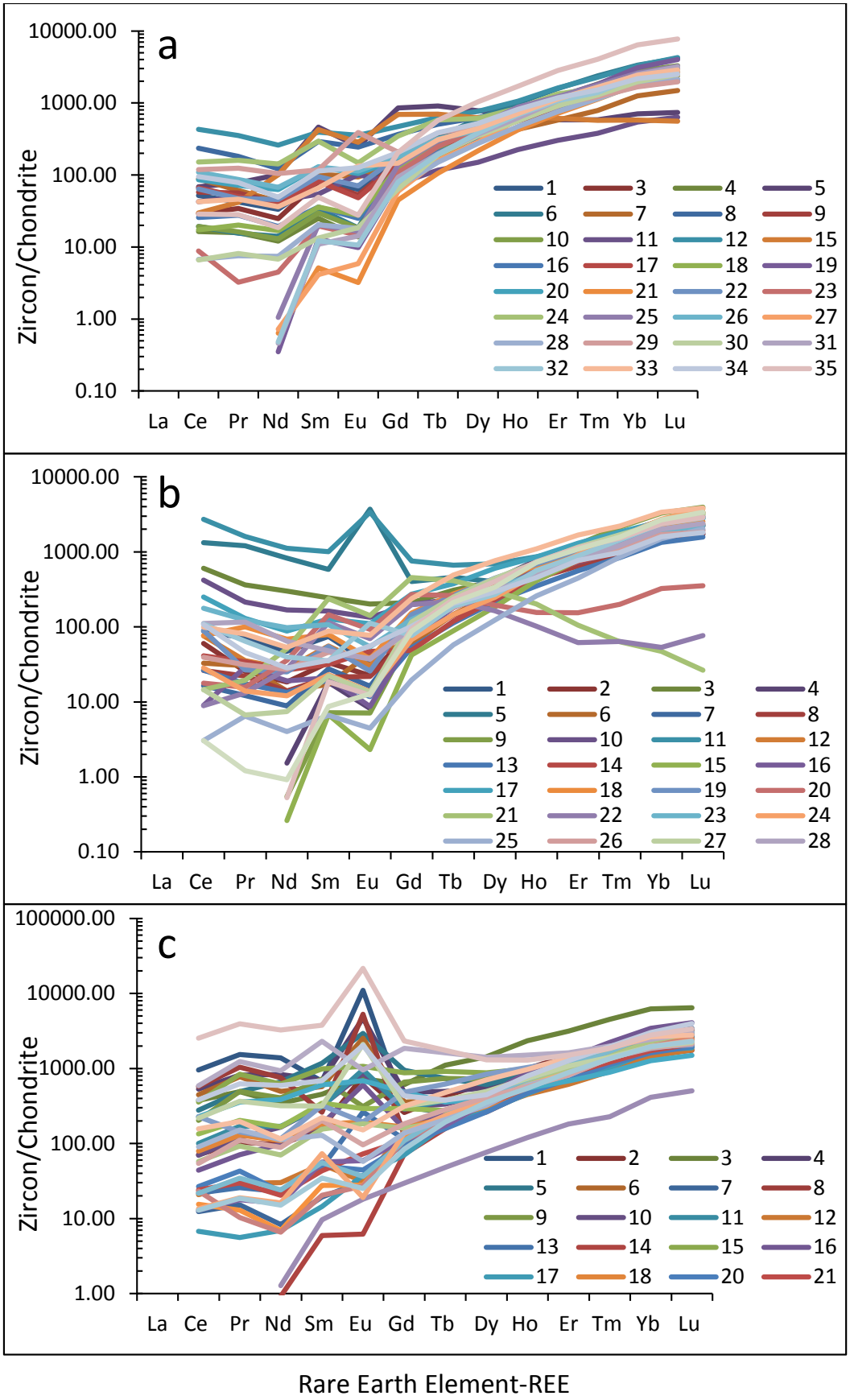

Figure 5. a - REE pattern of zircon grains from sample CMR06 showing negative Eu anomaly with HREE enrichment also observe are some grains with LREE enrichment, negative Eu anomaly with relatively stable HREE (5 and 15) whereas grains 11 and 29 show positive Eu anomaly with HREE enrichment. b - REE patterns of zircon grains for CMR07 showing high Ce concentrations, negative Eu anomaly and HREE enrichment. Discrepancy patterns for grains 5, 11, 29 with positive Eu anomalies followed by HREE enrichment and grains 20, 21, and 22 with negative Eu anomaly and HREE depletion can also be observed. c - REE patterns of zircon grains for CMR08, showing great variation in patterns with HREE enrichment, positive Eu anomaly, negative Eu anomaly and grains showing progressive enrichment from LREE to HREE

Table 2. Trace and Rare Earth Element composition of zircon grains form the investigated Bétaré Oya granitoid

	Ce	Pr	Nd	Sm	Eu	Gd	Tb	Dy	Ho	Er	Tm	Yb	Lu	Ti	Y	U	Th	Th/U	Hf	Eu/Eu*	Ce/Sm	Yb/Gd	U/Ce
CMR06																							
06Z1	51.7	42	33.5	80.4	63.2	173	314	472	712	944	1328	1783	2033	10.9	1077	1217	166	0.14	12300	0.5	0.6	10.3	23.5
06Z3	29	34.3	24.7	80.4	52	138	255	419	707	1063	1741	2658	2967	27.1	1199	1335	179	0.13	13000	0.5	0.4	19.2	46
06Z4	16.3	15.8	12	25	13.9	92	198	369	632	875	1296	1938	2407	1.7	964	1903	234	0.12	11500	0.3	0.7	21	117
06Z5	68.4	78.1	101	461	248.7	854	911	780	736	583	583	709	740	18.5	1190	801	860	1.09	8680	0.4	0.1	0.8	11.7
06Z6	19.2	15.5	14	33.8	18.5	161	327	610	1002	1594	2385	3366	4150	4.4	1761	1611	180	0.12	11670	0.3	0.6	20.9	83.7
06Z7	88.1	60.9	42.9	103	93.8	149	170	358	432	581	785	1255	1488	24.1	656	969	279	0.31	11900	0.8	0.9	8.4	11
06Z8	237	181	123	291	245.1	367	507	630	786	1000	1239	1714	2008	33.2	1350	1363	615	0.5	10140	0.7	0.8	4.7	5.8
06Z9	57.9	56	40.3	81.1	52.8	150	211	394	641	963	1457	2093	2634	8.6	1025	1116	70	0.07	11900	0.5	0.7	13.9	19.3
06Z10	19.2	16.3	12.9	29.7	18.3	93	217	402	722	1175	1830	2789	3309	5.2	1235	2132	122	0.07	12910	0.3	0.6	29.8	111
06Z11	42.6	49.6	43.8	54.1	101.2	76	117	150	225	302	381	543	634	18.7	359	508	89	0.18	11680	1.6	0.8	7.2	11.9
06Z12	431	355	261	395	355.2	472	629	764	1055	1613	2271	3298	4268	158	1790	1433	141	0.1	13500	0.8	1.1	7	3.3
06Z15	29.7	41.9	101	426	284.2	693	701	622	652	611	575	578	561	10.6	1006	760	637	0.84	9910	0.5	0.1	0.8	25.6
06Z16	25.8	27.7	19.3	35.8	25	92	205	335	586	969	1506	2398	2902	1.9	1100	1175	159	0.12	13400	0.4	0.7	25.9	45.6
06Z17	65.9	50.2	39.8	81.1	48.1	142	258	374	562	794	1308	1783	2102	8.2	924	1432	174	0.12	12540	0.4	0.8	12.5	21.7
06Z18	17.3	20.2	16.8	35.8	27.7	127	269	439	734	1138	1615	2391	2728	12.2	1131	1847	227	0.12	12600	0.4	0.5	18.8	107
06Z19	3.3	bdl	0.4	12.8	9.8	81	192	365	672	1219	1814	3099	4012	2.7	1247	1800	78	0.04	12240	0.3	0.3	38.3	538
06Z20	86.1	71.9	62.6	130	104.8	167	292	467	679	1000	1636	2124	2459	13.9	1106	1399	160	0.11	12070	0.7	0.7	12.7	16.2
06Z21	1.2	bdl	0.6	5.1	3.2	45	106	216	423	721	1130	1814	2463	1.8	717	859	36	0.04	13680	0.2	0.2	40.6	712
06Z22	63.6	47.1	45.7	94.6	70.2	182	307	431	619	888	1287	1795	2122	15.4	1110	622	344	0.51	12680	0.5	0.7	9.8	9.8
06Z23	8.8	3.2	4.5	19.6	14.6	108	248	431	665	1050	1457	2224	2695	3.8	1165	1687	190	0.11	12610	0.3	0.5	20.7	191
06Z24	152	159	142	295	147.4	347	582	612	842	1344	1603	2484	2699	47	1369	1600	399	0.25	12850	0.5	0.5	7.2	10.5
06Z25	4.9	bdl	1.1	20.3	16.5	138	299	481	877	1225	1765	2615	3232	2.6	1384	1150	114	0.1	11570	0.3	0.2	19	234
06Z26	110	86.3	67.6	128	114	180	316	417	712	1113	1656	2398	2764	12.5	1138	1016	117	0.11	12800	0.8	0.9	13.3	9.2
06Z27	2.4	bdl	0.7	4.1	5.9	59	158	287	590	913	1429	2168	2650	1.6	935	929	54	0.06	13090	0.4	0.6	36.6	380
06Z28	6.7	7.5	7.4	20.3	18.1	68	150	274	473	763	1146	1789	2114	3.4	766	973	79	0.08	12900	0.5	0.3	26.4	145
06Z29	119	124	104	118	390.8	209	382	488	674	969	1223	1683	1963	98	1029	753	124	0.17	12680	2.5	1	8.1	6.3
06Z30	6.6	8.1	6.8	13.3	18.7	64	190	350	566	919	1287	1969	2484	4.1	920	1544	121	0.08	13400	0.6	0.5	30.9	234
06Z31	2.6	bdl	0.5	10.9	14.2	93	196	368	625	1075	1538	2484	3175	3.1	1101	1081	92	0.09	12420	0.4	0.2	26.6	409
06Z32	4.1	bdl	0.5	12.2	10.7	80	194	382	685	1075	1401	2342	2858	2.8	1120	3540	192	0.05	16100	0.3	0.3	29.3	868
06Z33	42.7	46.3	36.3	66.2	133.2	146	307	441	711	1138	1660	2416	2878	9.7	1133	1378	180	0.13	12500	1.4	0.6	16.6	32.2
06Z34	94.6	78.7	49	114	126.1	207	388	520	817	1175	1522	2180	2520	28	1310	1034	269	0.24	11760	0.8	0.8	10.6	10.9
06Z35	28.5	28.2	18.6	49.3	27.7	206	573	1045	1703	2825	4045	6398	7764	9.9	3160	4220	181	0.04	15900	0.3	0.6	31.1	148
	Ce	Pr	Nd	Sm	Eu	Gd	Tb	Dy	Ho	Er	Tm	Yb	Lu	Ti	Y	U	Th	Th/U	Hf	Eu/Eu*	Ce/Sm	Yb/Gd	U/Ce
CMR07																							
07Z1	88.1	71.1	47	74.3	32.7	136	238	357	643	906	1211	1758	2199	5.5	919	1592	221	0.14	11500	0.3	1.2	13	18.1
07Z2	60.4	25.5	18.4	33.5	22.4	90	209	332	593	916	1267	2012	2256	9.7	926	1728	171	0.1	13160	0.4	1.8	22.4	28.6
07Z3	604	363	300	243	200.7	210	307	407	584	975	1482	2453	3171	89	1038	2690	333	0.11	17100	0.9	2.5	11.7	4.5
07Z4	5.3	bdl	1.5	18.2	8.2	95	238	423	767	1125	1709	2646	2992	2.5	1370	1989	175	0.09	13190	0.2	0.3	27.7	376
07Z5	1321	1207	825	581	3694.5	402	460	398	548	813	1332	2323	2846	25.8	1010	4740	155	0.03	16300	7.6	2.3	5.8	3.6
07Z6	33	30.4	14	17.2	43.9	60	147	278	502	794	1494	2460	3333	4.4	1040	NA	NA	NA	14900	1.4	1.9	41.1	NA
07Z7	16.5	12.2	8.8	27.7	16.2	85	205	293	533	709	1057	1453	1711	3.8	814	1048	234	0.23	12500	0.3	0.6	17	63.6
07Z8	26.3	22	14	21.4	21.8	75	143	226	445	650	899	1398	1732	3	700	1325	119	0.09	11200	0.5	1.2	18.7	50.4
07Z9	3.5	bdl	0.5	7.2	7.1	79	189	356	716	1256	2130	3298	3943	3.9	1270	1611	77	0.05	14400	0.3	0.5	41.5	466
07Z20	17.8	15.6	35.7	145	93	269	260	195	156	154	200	325	354	6.5	314	538	137	0.26	12400	0.5	0.1	1.2	30.3
07Z21	14.5	19.4	51.2	238	142	454	413	301	201	106	64	47	26	9.6	344	355	193	0.56	8570	0.4	0.1	0.1	24.5
07Z22	8.9	13.1	27.4	114	70	198	219	164	101	62	64	53	76	9	180	220	80	0.37	9900	0.5	0.1	0.3	24.7
07Z23	177	123	97.2	107	54	125	219	315	531	813	1211	1882	2240	8.7	906	1617	146	0.09	14100	0.5	1.6	15	9.2
07Z24	28.2	14	12	23	14	68	145	248	509	917	1571	2708	3732	5.8	1057	2990	143	0.05	14470	0.3	1.2	39.9	106
07Z25	3.1	6.5	4	6.6	4	20	58	123	260	447	850	1491	2024	2.6	502	1571	59	0.04	15500	0.4	0.5	76.1	515
07Z26	39.3	31.3	27.1	45.9	38	94	180	305	480	763	1073	1708	1833	2	806	1313	131	0.1	11820	0.6	0.9	18.1	33.4
07Z27	14.6	6.7	7.4	22.3	13	116	249	441	727	1150	1692	2429	3175	4.4	1210	2182	302	0.14	12900	0.3	0.7	21	150
07Z28	111	116	64.3	48	37	95	201	309	474	800	1219	2006	2390	5.2	912	979	95	0.09	12030	0.5	2.3	21	8.8
07Z29	109	64.7	39.8	35.1	112	77	188	270	564	881	1441	2360	2846	14.5	985	1322	74	0.06	13030	2.2	3.1	30.7	12.1
07Z30	98.9	79.7	53.4	87.8	77	237	490	764	1095	1681	2215	3366	3850	2.2	1670	1772	696	0.39	12600	0.5	1.1	14.2	17.9
07Z33	107	45.5	28.4	35.8	56	102	204	296	454	766	980	1584	1813	15.9	835	1325	173	0.13	11190	0.9	3	15.5	12.3
07Z34	4	bdl	0.5	18.6	12	94	233	402	738	1138	1518	2366	2894	1.5	1244	835	78	0.09	11400	0.3	0.2	25	210
07Z35	3.1	1.2	0.9	8.6	13	87	212	337	725	1088	1579	2677	3362	5.9	1144	1020	64	0.06	11840	0.5	0.4	30.8	334

	Ce	Pr	Nd	Sm	Eu	Gd	Tb	Dy	Ho	Er	Tm	Yb	Lu	Ti	Y	U	Th	Th/U	Hf	Eu/Eu*	Ce/Sm	Yb/Gd	U/Ce
CMR08																							
08Z1	958	1541	1381	676	11030	310	258	333	524	850	1320	1845	2370	7.3	945	1615	120	0.07	13510	24.1	1.4	5.9	1.7
08Z2	70.8	104.5	96.3	163	782	259	427	642	1002	1488	2049	2975	3248	13.1	1600	2002	292	0.14	11960	3.8	0.4	11.5	28.3
08Z3	377	492	344	453	734	608	1102	1439	2344	3138	4534	6211	6463	12.4	3480	2630	403	0.15	13400	1.4	0.8	10.2	7
08Z4	532	821	829	699	4689	482	496	553	764	1081	1623	2491	2797	17.3	1252	1910	148	0.08	13000	8.1	0.8	5.2	3.6
08Z5	277	492	667	1176	2931	950	737	610	839	1144	1474	2441	2793	14.7	1336	899	82	0.09	12320	2.8	0.2	2.6	3.2
08Z6	447	776	495	574	2540	357	380	480	665	1044	1429	2280	2508	16.1	1160	1505	108	0.07	13530	5.6	0.8	6.4	3.4
08Z7	12.4	15.2	8.3	19.5	31	115	260	455	758	1300	1915	2901	3419	3.6	1433	1336	122	0.09	11340	0.7	0.6	25.2	108
08Z8	574	1045	757	262	5293	128	191	264	473	682	992	1547	1756	2.4	706	1508	147	0.1	11900	28.9	2.2	12.1	2.6
08Z9	204	496	405	723	311	658	740	728	989	1231	1510	2137	2130	146	1500	951	256	0.26	11400	0.5	0.3	3.2	4.7
08Z10	69.7	120	166	318	863	303	335	447	705	1113	1587	2540	2935	5.6	1174	1434	83	0.05	12700	2.8	0.2	8.4	20.6
08Z11	99.8	170	170	311	961	287	377	437	711	994	1441	2230	2626	5.8	1174	1484	181	0.12	12680	3.2	0.3	7.8	14.9
08Z12	20.7	29.4	30.2	52.7	31	144	224	293	451	613	915	1441	1760	3.5	741	1226	178	0.14	15060	0.4	0.4	10	59.2
08Z13	21.9	25.9	22.8	48.6	265	114	252	395	663	1069	1474	2199	2671	3.3	1177	2483	353	0.14	12300	3.6	0.4	19.4	114
08Z14	3.7	bdl	0.9	5.9	6	72	158	295	491	763	1170	1826	1931	0.8	913	2184	241	0.11	11900	0.3	0.6	25.2	590
08Z15	357	841	621	993	1066	879	911	874	993	1226	1733	2398	2915	34.7	1630	2570	243	0.09	13200	1.1	0.4	2.7	7.2
08Z16	43.9	71.1	98.5	182	604	156	271	435	894	1369	2223	3429	4065	3.3	1470	3311	236	0.07	14100	3.6	0.2	21.9	75.5
08Z17	6.8	5.6	7	14.5	38	70	177	270	463	736	1024	1714	1890	4.2	754	1522	158	0.1	12400	1.2	0.5	24.4	225
08Z18	79.1	129	109	182	194	165	214	313	504	741	1194	1820	2053	8.3	805	1390	106	0.07	11990	1.1	0.4	11	17.6
08Z20	26.6	43.1	22.8	50	44	95	158	264	474	713	1138	1615	1951	6.9	730	3590	294	0.08	11600	0.6	0.5	17	135
08Z21	24.1	30	20.4	43.2	73	110	200	329	551	844	1215	1733	2114	6.6	885	2172	155	0.09	13320	1.1	0.6	15.7	90
08Z22	134	204	166	345	291	291	274	381	595	931	1474	2354	2907	41	1105	3888	213	0.07	14790	0.9	0.4	8.1	29.1
08Z23	12.9	17.8	16	56.8	59	112	174	348	560	944	1368	2354	2947	6.9	991	923	196	0.28	10170	0.7	0.2	21	71.6
08Z24	228	358	385	605	686	487	357	398	546	681	891	1273	1500	29.2	872	1644	172	0.13	13100	1.3	0.4	2.6	7.2
08Z25	15.5	12.9	6.9	27.7	28	118	213	378	747	1094	1514	2199	2496	5.6	1144	1215	93	0.09	12020	0.5	0.6	18.6	78.4
08Z26	228	142	116	321	194	482	620	841	1033	1275	1538	1938	2057	51	1530	828	498	0.54	11200	0.5	0.7	4	3.6
08Z27	23.3	10.3	6.6	20.5	27	110	208	447	692	1044	1360	2081	2402	5.3	1053	1475	123	0.1	11960	0.6	1.1	18.9	63.2
08Z28	57.6	92.7	70.2	155	183	160	200	341	621	951	1449	2298	3012	28.4	1047	2870	267	0.11	15280	1.2	0.4	14.4	49.8
08Z35	219	366	319	316	2096	315	380	496	734	1075	1405	1963	2220	11.7	1147	1535	178	0.12	10960	6.6	0.7	6.2	7
08Z36	587	1239	932	2311	952	1864	1612	1415	1516	1613	1996	2453	2955	148	2380	842	105	0.12	11370	0.5	0.3	1.3	1.4
08Z37	12.9	18.6	15.1	34.5	25	84	194	354	546	881	1344	1950	2309	2.7	978	1635	128	0.08	11800	0.5	0.4	23.1	127
08Z38	157	197	115	222	151	314	479	707	969	1400	1866	2640	2801	15	1620	1730	229	0.13	12000	0.6	0.7	8.4	11
08Z39	383	625	595	689	2025	432	380	447	797	1269	1960	3012	3992	26.2	1471	1566	273	0.17	11700	3.7	0.6	7	4.1
08Z40	2545	3955	3260	3777	21670	2332	1751	1301	1291	1513	1883	2795	3374	78	2240	2240	431	0.19	13100	7.3	0.7	1.2	0.9

4.3. U-Pb and Hf Isotopes Data

U-Pb data for the various samples are presented in Table 3. A total of 103 zircon grains were analyzed: CMR06 = 32 grains, CMR07 = 33 grains and CMR08 = 38 grains. This result show varying concentrations of U, Pb, Th and Th/U ratio. Sample CMR06 shows, U (508 - 4220 ppm), Pb (11 - 235 ppm), Th (47 - 399 ppm) and a Th/U ratio range of 0.04 - 1.1. Sample CMR07 reveals, U concentrations between 220 and 4740 ppm, Pb (19 - 212 ppm), Th (47 - 333 ppm) and a Th/U ratio between 0.03 - 0.26. CMR08 values vary for U (242 - 3590 ppm), Pb (2 - 192 ppm), Th (9 - 498 ppm) and a Th/U ratio range of 0.04 - 0.28. On the discriminant plots of [3], the Bétaré Oya samples reveal a granodioritic composition (Figure 6a, Figure 6b). Their Th/U ratios and Ce/Sm vs Yb/Gd plots indicate that the granitoids originated from the crust (Figure 6c, Figure 6d). U-Pb data were plotted with the aid of isoplot and concordia obtained as presented in Figure 7. Sample CMR06 has an upper intercept at 1838± 1000 Ma with a lower intercept at 587±100 Ma and a mean age of 635.1±5.7Ma (MSWD=6.7). CMR08 has an upper intercept at 879 ± 580 Ma, lower intercept at -10 ± 2100 Ma and a mean age of 633.1±4.5Ma (MSWD=15) whereas CMR07 intercept the isochron line at a single point with intercept at 651.7±7.3 (MSWD=13). It shows a mean age of 633.2±5.3 Ma. Hafnium concentrations vary from 6560 ppm to 17100 ppm. The lowest Hf concentration is observed in CMR08 which ranges from 6560 ppm to 15280 ppm with an average value of 12244 ppm. Sample CMR07 has Hf values ranging from 8570 to 17100 ppm with an average value of 12823 ppm whereas those of CMR06 range from 8680 to 16100 ppm with an average 12465 ppm. $^{176}Hf/^{177}Hf$ ratio is 0.28 for all analyzed samples while $^{176}Lu/^{177}Hf$ ratios are quiet low ranging from 0.0 to 0.002. εHf_t are significantly negative to positive ranging from -5.29 to 13.62. Hf model ages were also calculated and vary from 1010 - 1390 Ma for CMR06, 680 -1415 Ma for CMR07 and 964 -1425 Ma for CMR08 (Table 4).

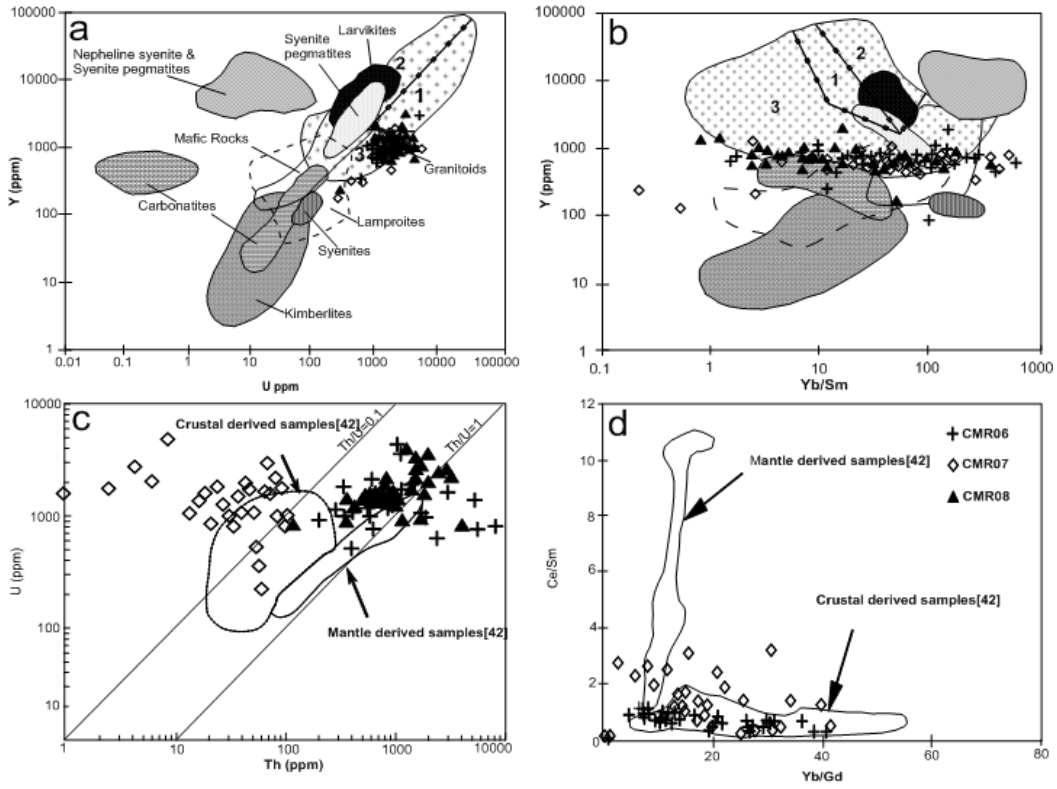

Figure 6. REE discriminant diagrams for zircons. a - Y vs U in ppm and b -Y in ppm vs Yb/Gd jointly characterise the type of granitoid as a granodiorite and tonalite after [3] where 1 = Aplites leucogranite, 2 = granites and 3 = granodiorites and tonalites. c - U vs Th in ppm. d - Ce/Sm vs Yb/Gd chracterise the source of the granitoid as crustal after [42]

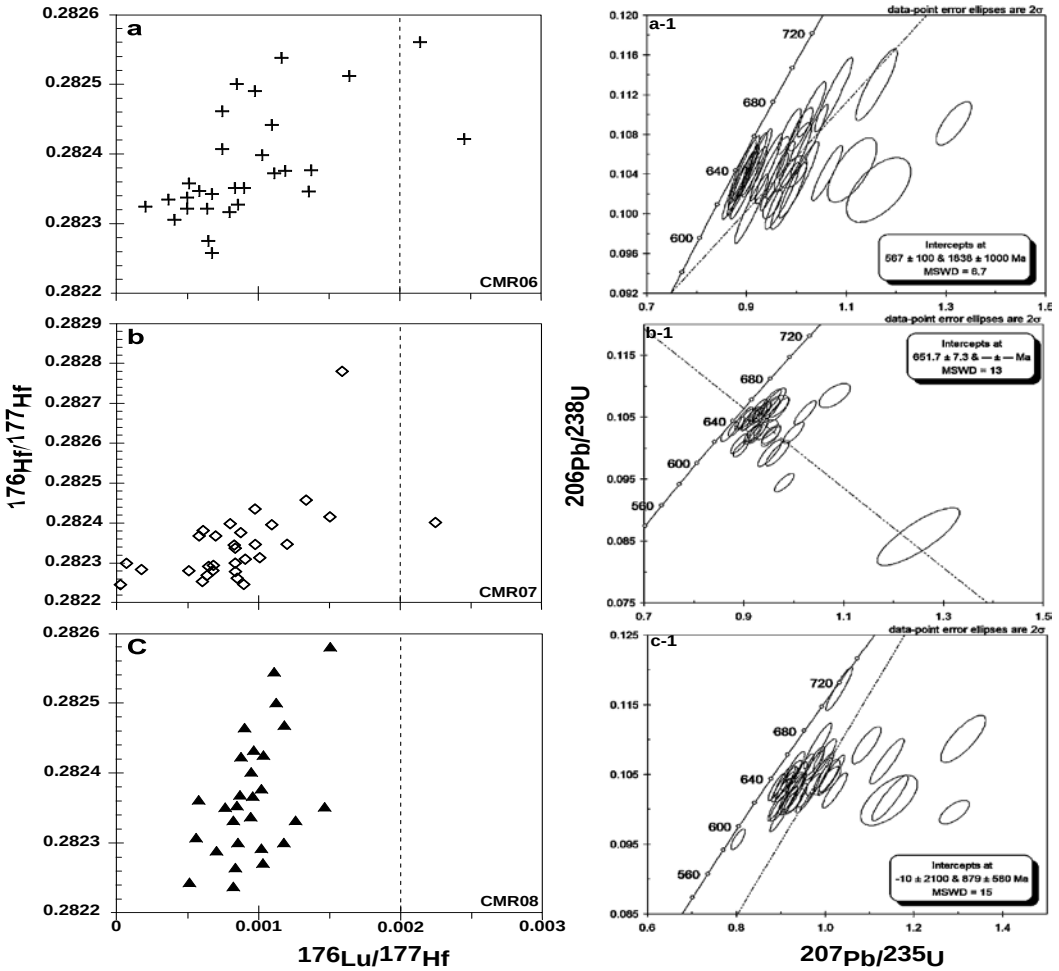

Figure 7. $^{176}Lu/^{177}Hf$ and $^{176}Hf/^{177}Hf$ isotope variations in three granitic samples from the Bétaré-Oya gold district and their corresponding concordia diagrams. $^{176}Lu/^{177}Hf$ ratios generally < 0.002

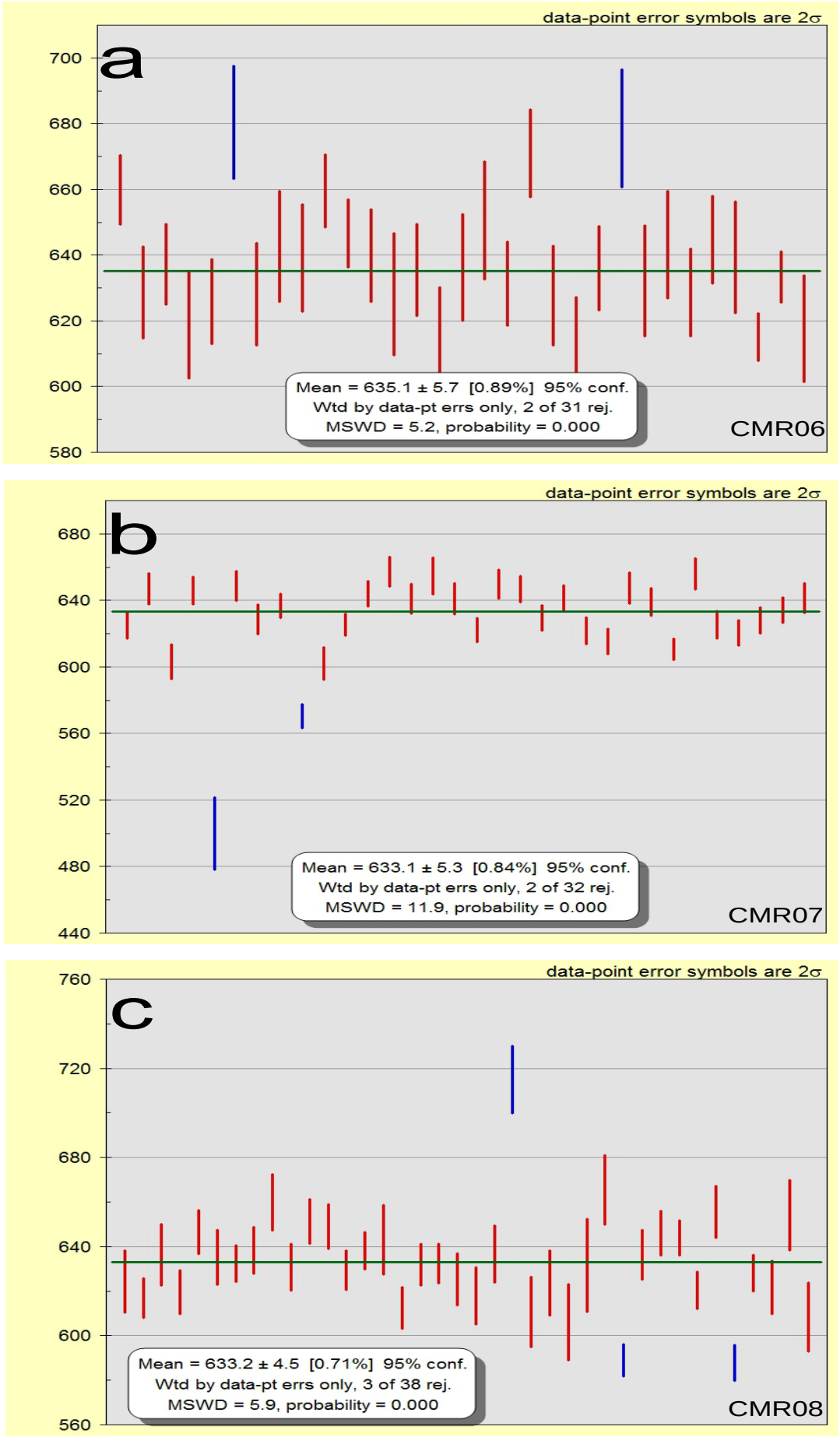

Figure 8. Histograms of 207Pb corrected 206Pb/238U ages for the granitoid samples revealing Pan African mean ages of 635.1±5.7Ma for CMR06 (a); 633.1±5.3Ma for CMR07 (b) and 633.2±4.5Ma (c)

Table 3. Zircon U-Pb analytical data by LA ICP-MS

	Pb (ppm)	U (ppm)	Th (ppm)	Th/U	$^{207}Pb/^{206}Pb$	2 s. %	$^{207}Pb/^{235}U$	2 s. %	$^{206}Pb/^{238}U$	2 s. %	Rho	$^{207}Pb/^{206}Pb$ (Ma)	2 SE abs.	$^{206}Pb/^{238}U$ (Ma)	2 SE abs.	Ref age	207Pb corr'd 206/238 (Ma)	2 SE abs.
CMR06																		
06Z1	63	1217	165.9	0.141	0.06706	1.047	1.009	1.95	0.1085	1.645	0.84	839	21.8	664	10.92	664	659.82	10.6
06Z3	58.9	1335	179	0.13	0.06685	0.819	0.956	2.43	0.1032	2.284	0.94	832.8	17.1	633	14.46	633	628.6	14
06Z4	67.8	1903	234.3	0.124	0.06344	1.022	0.916	2.23	0.1042	1.983	0.89	725	21.7	639	12.67	639	637.12	12.3
06Z5	234.7	801	860	1.087	0.06902	1.126	0.972	2.92	0.1018	2.699	0.92	898	23.2	625	16.87	625	618.69	16.3
06Z6	50.2	1611	179.6	0.118	0.06185	0.837	0.876	2.28	0.1021	2.117	0.93	668.6	17.9	627	13.27	627	625.8	12.9
06Z7	131.4	969	279	0.312	0.0744	1.355	1.161	2.95	0.113	2.615	0.89	1050	27.3	690	18.04	690	680.41	17.3
06Z8	239	1363	615	0.504	0.0768	2.585	1.112	3.62	0.1044	2.54	0.7	1108	51.6	640	16.26	640	628.15	15.6
06Z9	43.3	1116	70.1	0.072	0.06775	1.513	0.993	3.09	0.1057	2.696	0.87	859	31.4	647	17.44	647	642.72	16.9
06Z10	59.7	2132	122.1	0.068	0.06466	0.934	0.94	2.79	0.1047	2.627	0.94	763	19.7	642	16.86	642	639.16	16.3
06Z11	27.89	508	88.7	0.177	0.06581	0.956	0.986	1.98	0.1083	1.736	0.88	800	20	663	11.51	663	659.62	11.1
06Z12	138.8	1433	140.8	0.099	0.0882	1.455	1.316	2.19	0.1091	1.636	0.75	1385	27.9	667	10.92	667	646.64	10.3
06Z15	191.5	760	637	0.841	0.06219	0.892	0.893	2.43	0.1045	2.257	0.93	680	19.1	641	14.47	641	639.85	14
06Z16	76	1175	159	0.118	0.06916	1.093	1.005	3.23	0.1034	3.039	0.94	903	22.5	634	19.27	634	628.05	18.6
06Z17	63.4	1432	173.5	0.121	0.06716	0.865	0.968	2.42	0.1044	2.259	0.93	842.5	18	640	14.46	640	635.48	14
06Z18	76	1847	227.3	0.124	0.0657	1.005	0.91	3	0.1005	2.831	0.94	799	21.1	617	17.46	617	613.43	16.9
06Z19	29.2	1800	78.2	0.044	0.06612	1.322	0.952	2.95	0.1044	2.634	0.89	812	27.7	640	16.86	640	636.27	16.3
06Z20	72.1	1399	159.7	0.113	0.06979	0.894	1.026	2.98	0.1073	2.84	0.95	922	18.4	657	18.66	657	650.59	18
06Z21	11.48	859	35.77	0.042	0.0625	0.908	0.888	2.29	0.1031	2.097	0.92	691	19.4	632	13.26	632	631.28	12.9
06Z22	119	622	344	0.505	0.06794	0.981	1.031	2.28	0.1105	2.053	0.9	866	20.3	676	13.88	676	670.93	13.4
06Z23	57.2	1687	190.3	0.114	0.06331	0.863	0.897	2.63	0.1026	2.487	0.94	718.5	18.3	629	15.65	629	627.69	15.2
06Z24	176.2	1600	399	0.249	0.0831	3.687	1.165	4.5	0.1024	2.588	0.57	1254	71.9	628	16.25	628	611.71	15.6
06Z25	34.22	1150	113.5	0.097	0.06248	0.798	0.897	2.23	0.1039	2.082	0.93	690.5	17	637	13.26	637	636.06	12.9
06Z26	56	1016	116.5	0.114	0.06944	1.01	1.075	2.91	0.112	2.725	0.94	913	20.8	684	18.64	684	678.57	18
06Z27	17.01	929	53.9	0.058	0.06285	0.857	0.893	2.89	0.1033	2.756	0.95	704.4	18.2	633	17.45	633	632.21	17
06Z28	27.28	973	79.1	0.082	0.06338	0.895	0.92	2.76	0.1052	2.615	0.95	721	19	645	16.87	645	643.11	16.4
06Z29	61.1	753	123.9	0.167	0.07383	0.95	1.062	2.37	0.1041	2.172	0.92	1038	19.2	638	13.86	638	628.64	13.3
06Z30	36.37	1544	121	0.08	0.06287	0.821	0.916	2.3	0.1054	2.146	0.93	703.7	17.5	646	13.87	646	644.69	13.5
06Z31	26.92	1081	92.4	0.087	0.06211	0.816	0.895	2.85	0.1044	2.728	0.96	677.6	17.4	640	17.46	640	639.32	17
06Z32	72	3540	192.2	0.055	0.0693	3.403	0.82	29.1	0.083	28.92	0.99	1040	70.1	510	147.5	510	506.77	143
06Z33	60	1378	179.9	0.131	0.06754	1.14	0.952	1.65	0.101	1.198	0.72	853	23.7	620.4	7.435	620	615.04	7.19
06Z34	95.2	1034	269	0.236	0.0685	1.906	0.994	2.28	0.1042	1.255	0.55	887	39.4	638.8	8.02	639	633.28	7.79
06Z35	93	4220	181	0.038	0.07053	1.244	0.985	2.97	0.1018	2.699	0.91	943	25.5	625	16.87	625	617.56	16.2
CMR07																		
07Z1	71.7	1592	221.3	0.143	0.06485	0.971	0.9181	1.6	0.1023	1.275	0.8	769	20.4	627.9	8.007	628	624.76	7.76
07Z2	64.1	1728	170.5	0.102	0.06593	0.965	0.97	1.78	0.1062	1.498	0.84	806	20.2	650.8	9.751	651	647.08	9.44
07Z3	61.2	2690	333	0.115	0.06925	1.041	0.952	2.07	0.0992	1.785	0.86	905	21.5	609.6	10.88	610	603.12	10.5
07Z4	60.1	1989	174.9	0.089	0.06435	0.917	0.9358	1.61	0.1058	1.327	0.82	753	19.4	648.1	8.597	648	645.93	8.34
07Z5	376	4740	154.5	0.033	0.1053	3.038	1.25	5.4	0.0857	4.462	0.83	1719	55.8	530	23.65	530	499.95	21.8
07Z7	75.5	1048	234.2	0.23	0.06306	0.834	0.928	1.64	0.1061	1.411	0.86	710	17.7	650.3	9.176	650	648.71	8.91
07Z8	44.4	1325	119.4	0.094	0.06534	1.039	0.93	1.78	0.103	1.448	0.81	784	21.8	632.1	9.155	632	628.55	8.87
07Z9	24.08	1611	76.6	0.049	0.06399	0.976	0.9222	1.52	0.1042	1.168	0.77	741	20.7	638.8	7.462	639	636.7	7.25
07Z10	38.7	834	72.6	0.088	0.07535	1.001	0.981	1.62	0.0944	1.268	0.78	1077	20.1	581.3	7.371	581	570.42	7.06
07Z11	63.6	1798	121.7	0.069	0.07072	1.05	0.968	1.99	0.0992	1.689	0.85	949	21.5	609.4	10.29	609	602.06	9.91
07Z12	68.5	1262	208.3	0.172	0.06481	0.843	0.917	1.38	0.1024	1.097	0.79	767.9	17.8	628.4	6.894	628	625.38	6.69
07Z13	24.7	1014	70.6	0.071	0.06368	0.988	0.929	1.59	0.1054	1.243	0.78	730	20.9	647.3	8.049	647	644.07	7.8
07Z14	20.33	784	52.1	0.069	0.06433	0.936	0.955	1.68	0.1077	1.393	0.83	752	19.8	659.3	9.182	659	657.22	8.91
07Z15	15.34	1474	46.9	0.033	0.063	0.834	0.915	1.65	0.1048	1.426	0.86	708.1	17.7	642.5	9.165	643	641.02	8.9
07Z16	24.2	1083	55.4	0.053	0.06511	1.118	0.96	2.08	0.1074	1.749	0.84	777	23.5	657	11.49	657	654.83	11.1
07Z17	185.8	1960	494	0.262	0.06997	0.886	1.023	1.75	0.1057	1.505	0.86	927	18.2	647.5	9.742	648	641.02	9.39
07Z18	123.9	1729	332.2	0.197	0.06747	1.097	0.955	1.62	0.1022	1.187	0.73	854	22.8	628.3	7.457	628	622.21	7.2
07Z19	47.4	1071	112.8	0.109	0.0663	1.821	0.963	2.3	0.1067	1.404	0.61	811	38.1	653.6	9.177	654	649.76	8.92
07Z20	45.04	538	137	0.258	0.06416	1.027	0.937	1.61	0.1059	1.239	0.77	746	21.7	648.8	8.036	649	646.67	7.8
07Z21	59.3	355.2	193	0.556	0.06165	0.941	0.871	1.58	0.1027	1.271	0.8	661	20.2	631.2	8.022	631	629.53	7.79
07Z22	25.3	220	79.9	0.37	0.06257	0.975	0.906	1.58	0.1048	1.249	0.79	695	20.8	642.7	8.03	643	641.35	7.81
07Z23	75	1617	145.8	0.093	0.07044	0.967	1	1.67	0.1025	1.363	0.82	940	19.8	628.9	8.574	629	621.77	8.26
07Z24	42.9	2990	142.6	0.049	0.06464	0.899	0.891	1.57	0.1007	1.292	0.82	762	18.9	618.6	7.994	619	615.4	7.75
07Z25	22.8	1571	59	0.038	0.06497	1.031	0.951	1.82	0.1061	1.5	0.82	773	21.7	651.5	9.77	652	647.23	9.45
07Z26	42.92	1313	130.9	0.1	0.06342	0.82	0.912	1.57	0.1045	1.341	0.85	722.1	17.4	640.5	8.587	641	638.92	8.34
07Z27	90.6	2182	301.6	0.141	0.06486	0.873	0.894	1.39	0.09993	1.083	0.78	769.3	18.4	614	6.65	614	610.66	6.45
07Z28	55.6	979	94.9	0.092	0.072	1.828	1.082	2.35	0.1085	1.47	0.63	983	37.2	663.9	9.76	664	655.93	9.42
07Z29	28.69	1322	73.6	0.057	0.06556	0.822	0.928	1.59	0.1025	1.363	0.86	792.3	17.2	628.8	8.572	629	625.42	8.3
07Z30	211.6	1772	696	0.395	0.06757	1.054	0.954	1.66	0.1019	1.279	0.77	855	21.9	625.7	8.005	626	620.36	7.74
07Z33	60.7	1325	172.6	0.132	0.06611	1.661	0.944	2.09	0.103	1.268	0.61	807	34.8	631.7	8.009	632	627.97	7.79
07Z34	22.31	835	77.9	0.093	0.06186	0.823	0.885	1.51	0.1035	1.263	0.84	669.1	17.6	634.7	8.014	635	634.14	7.8
07Z35	19.04	1020	64.3	0.062	0.0623	0.858	0.9	1.66	0.1048	1.426	0.86	684.2	18.3	642.2	9.16	642	641.55	8.91

	Pb (ppm)	U (ppm)	Th (ppm)	Th/U	$^{207}Pb/^{206}Pb$	2 s. %	$^{207}Pb/^{235}U$	2 s. %	$^{206}Pb/^{238}U$	2 s. %	Rho	$^{207}Pb/^{206}Pb$ (Ma)	2 SE abs.	$^{206}Pb/^{238}U$ (Ma)	2 SE abs.	Ref age	207Pb corr'd 206/238 (Ma)	2 SE abs.
CMR 08																		
08Z1	37.5	1615	119.6	0.073	0.06474	1.044	0.923	2.53	0.1022	2.305	0.91	765	22	627	14.45	627	624.25	14
08Z2	96.9	2002	292	0.143	0.06655	1.316	0.93	1.97	0.1012	1.471	0.75	822	27.5	621.3	9.139	621	616.96	8.85
08Z3	148.6	2630	403	0.153	0.06996	0.902	1.014	2.42	0.1049	2.249	0.93	927	18.5	643	14.46	643	636.3	13.9
08Z4	45.79	1910	147.9	0.076	0.06702	0.931	0.938	1.9	0.1017	1.651	0.87	838	19.4	624.4	10.31	624	619.58	9.96
08Z5	33.83	899	82.2	0.089	0.06663	0.933	0.975	1.84	0.1062	1.587	0.86	826	19.5	650.4	10.32	650	646.54	9.99
08Z6	54.4	1505	108.3	0.07	0.06912	1.404	1.003	2.42	0.1046	1.976	0.82	900	28.9	643	12.71	643	635.17	12.2
08Z7	41.5	1336	121.5	0.086	0.065	1.363	0.933	1.92	0.1036	1.351	0.7	772	28.7	635.2	8.58	635	632.37	8.33
08Z8	47.4	1508	147	0.095	0.06511	0.914	0.938	1.93	0.1046	1.7	0.88	778	19.2	641	10.9	641	638.22	10.6
08Z9	94.3	951	256	0.26	0.07223	1.361	1.093	2.41	0.1092	1.987	0.83	991	27.7	668	13.27	668	659.86	12.8
08Z10	32.71	1434	83.2	0.055	0.06395	0.893	0.91	1.94	0.1032	1.721	0.89	739	18.9	633	10.9	633	630.78	10.6
08Z11	77.9	1484	180.7	0.115	0.06585	0.928	0.977	1.83	0.1069	1.578	0.86	801	19.4	654.6	10.33	655	651.29	10
08Z12	81.9	1226	178.4	0.138	0.06366	0.959	0.933	1.85	0.1062	1.587	0.86	730	20.3	650.6	10.33	651	648.84	10
08Z13	129	2483	353.2	0.137	0.06333	0.827	0.898	1.67	0.1029	1.45	0.87	719	17.5	631.4	9.152	631	629.46	8.88
08Z14	99.2	2184	241.4	0.106	0.06374	0.968	0.9191	1.65	0.1044	1.342	0.81	732	20.5	641.5	8.608	642	638.08	8.34
08Z15	237.7	2570	243	0.09	0.07653	1.183	1.139	2.75	0.1069	2.483	0.9	1108	23.6	654	16.24	654	643	15.5
08Z16	104.8	3311	235.8	0.067	0.0647	1.002	0.896	1.87	0.1002	1.578	0.84	764	21.1	615.7	9.718	616	612.38	9.42
08Z17	74.8	1522	158.2	0.099	0.06253	0.835	0.891	1.75	0.1032	1.537	0.88	693.4	17.8	632.9	9.728	633	631.85	9.45
08Z18	100.4	1390	105.5	0.072	0.07058	1.371	1.011	1.98	0.1043	1.432	0.72	943	28.1	639.4	9.159	639	632.29	8.84
08Z20	171.7	3590	294.1	0.076	0.0675	0.92	0.964	2.13	0.1027	1.916	0.9	855	19.1	630	12.07	630	625.15	11.7
08Z21	103	2172	154.5	0.095	0.06375	0.832	0.896	2.29	0.101	2.138	0.93	734.5	17.6	620	13.26	620	617.84	12.9
08Z22	161.2	3888	213.3	0.071	0.06792	1.216	0.986	2.4	0.1047	2.067	0.86	867	25.2	642	13.27	642	636.68	12.8
08Z23	104.6	923	195.6	0.28	0.06318	0.855	1.032	2.35	0.1173	2.189	0.93	715.2	18.2	715	15.65	715	715.02	15.2
08Z24	104.2	1644	172.1	0.133	0.06541	0.835	0.907	2.78	0.1	2.648	0.95	787.2	17.5	614	16.26	614	610.67	15.7
08Z25	62.6	1215	93.4	0.095	0.06563	0.92	0.929	2.57	0.1022	2.401	0.93	794	19.3	627	15.05	627	623.58	14.6
08Z26	256	828	498	0.543	0.0821	3.492	1.144	4.54	0.1013	2.906	0.64	1236	68.4	622	18.08	622	606.04	17.3
08Z27	82.2	1475	123.3	0.101	0.06758	1.075	0.977	3.57	0.1038	3.409	0.95	855	22.3	636	21.68	636	631.61	20.9
08Z28	90.8	2870	267.4	0.112	0.06447	0.993	0.983	2.63	0.1091	2.435	0.93	756	21	667	16.24	667	665.41	15.8
08Z30	2.348	242.4	9.63	0.038	0.05997	1.026	0.804	1.62	0.0957	1.253	0.77	602	22.2	589.3	7.387	589	588.9	7.2
08Z31	40.7	1332	128	0.093	0.06298	1.092	0.909	2.11	0.104	1.802	0.86	707	23.2	638	11.49	638	636.28	11.2
08Z32	49.06	1495	149	0.099	0.06484	0.836	0.953	1.8	0.1059	1.591	0.89	768.8	17.6	648.5	10.32	649	646.15	10
08Z33	46.91	1424	148	0.102	0.06391	0.929	0.93	1.55	0.1054	1.243	0.8	738	19.7	645.9	8.032	646	643.89	7.8
08Z34	49.3	1366	149	0.109	0.06523	0.872	0.921	1.63	0.1016	1.374	0.84	781.5	18.3	623.9	8.571	624	620.32	8.3
08Z35	66.1	1535	177.9	0.117	0.06636	1.042	0.999	2.11	0.1077	1.834	0.87	817	21.8	659	12.08	659	655.63	11.7
08Z36	87	842	105.3	0.125	0.0936	1.578	1.291	2.11	0.0996	1.398	0.66	1497	29.8	612	8.554	612	587.73	8.06
08Z37	38.53	1635	128.1	0.077	0.06365	0.886	0.906	1.62	0.1027	1.361	0.84	730	18.8	630	8.574	630	628.03	8.32
08Z38	107.1	1730	229	0.131	0.07214	0.984	1.022	2.24	0.1027	2.011	0.9	992	20	630	12.67	630	621.67	12.2
08Z39	191.7	1566	273.4	0.175	0.0861	1.897	1.311	3.14	0.1101	2.503	0.8	1338	36.7	673	16.84	673	654.09	15.9
08Z40	171.8	2240	431	0.192	0.08143	1.246	1.146	2.89	0.1016	2.607	0.9	1231	24.4	623	16.24	623	608.29	15.4

Table 4. Lu/Hf isotopic composition of zircon grains from the Bétaré Oya granitoid

	Total Hf (V)	176Hf/177Hf	2SE	Hf178/177	2 SE	Lu176/Hf177	2 SE	176Yb/177Hf	2 SE	εHf (t)	2 SE	Ref age
CMR06												
06Z1	11.43	0.282322	0.000055	1.467324	0.000082	0.000498	0.000007	0.0193753	0.0004968	-15.91388	1.1	664
06Z3	12.18	0.282305	0.000081	1.46729	0.0001	0.000409	0.000024	0.0147739	0.0011349	-16.51507	1.62	633
06Z4	10.49	0.282338	0.000076	1.467302	0.000097	0.000499	0.000016	0.0197378	0.0012417	-15.34805	1.52	639
06Z5	9.99	0.282343	0.000063	1.467305	0.000073	0.000669	0.000031	0.0278595	0.0025068	-15.17123	1.26	625
06Z6	16.34	0.282347	0.000065	1.467244	0.000077	0.001357	0.000042	0.0405544	0.0014854	-15.02978	1.3	627
06Z7	12.06	0.282358	0.000065	1.467315	0.00008	0.000517	0.000006	0.0190295	0.0005276	-14.64077	1.3	690
06Z8	7.67	0.282421	0.000085	1.46732	0.0001	0.002447	0.000064	0.0928721	0.0016581	-12.41283	1.7	640
06Z9	10.44	0.282351	0.000068	1.467308	0.000094	0.000835	0.000005	0.0322185	0.0011365	-14.88832	1.36	647
06Z10	12.76	0.282373	0.000056	1.467293	0.000067	0.001115	0.000038	0.0365185	0.0005357	-14.11031	1.12	642
06Z11	5.54	0.282461	0.000089	1.46716	0.00012	0.000744	0.000014	0.0212493	0.0020276	-10.99826	1.78	663
06Z12	11.28	0.282351	0.000067	1.467245	0.00008	0.000898	0.000022	0.0338619	0.0008543	-14.88832	1.34	667
06Z15	9.477	0.282334	0.000075	1.467366	0.000094	0.000374	0.000003	0.015525	0.0003176	-15.48951	1.5	641
06Z16	5.97	0.282512	0.000093	1.46714	0.0001	0.00164	0.0001	0.0455408	0.0055666	-9.194687	1.86	634
06Z17	9.65	0.282489	0.000077	1.467209	0.000084	0.000983	0.000044	0.0300579	0.0025215	-10.00806	1.54	640
06Z18	8.76	0.282538	0.000073	1.46719	0.00011	0.00116	0.000038	0.0338305	0.0037731	-8.275218	1.46	617
06Z19	9.67	0.282325	0.000085	1.467324	0.000093	0.000209	0.000014	0.0100875	0.000839	-15.80779	1.7	640
06Z20	11.57	0.282372	0.000062	1.467297	0.000088	0.001195	0.000022	0.0460121	0.001956	-14.14567	1.24	657
06Z21	8.21	0.2825	0.00017	1.46702	0.00026	0.000851	0.000038	0.0234029	0.0015175	-9.619057	3.4	632
06Z22	9.85	0.282376	0.000077	1.46737	0.0001	0.00137	0.00015	0.0620121	0.0050432	-14.00422	1.54	676
06Z23	12.96	0.282322	0.000073	1.467286	0.000076	0.000639	0.000008	0.0254585	0.0010407	-15.91388	1.46	629
06Z24	11.147	0.282275	0.000072	1.46739	0.000095	0.000653	0.00001	0.0255829	0.0006454	-17.576	1.44	628
06Z25	11.046	0.282258	0.000073	1.467363	0.000072	0.000678	0.000013	0.0275692	0.0006538	-18.17719	1.46	637
06Z26	10.79	0.282317	0.000083	1.4673	0.00012	0.000796	0.000008	0.0315914	0.0008626	-16.0907	1.66	684
06Z27	11.76	0.282326	0.000071	1.467314	0.000087	0.000864	0.00001	0.0265235	0.0010131	-15.77242	1.42	633
06Z28	8.28	0.282408	0.000063	1.467299	0.000094	0.000749	0.000009	0.0214154	0.0022529	-12.87256	1.26	645
06Z29	11.8	0.282346	0.000085	1.46735	0.00013	0.000593	0.000014	0.0242408	0.00108	-15.06514	1.7	638
06Z30	13.86	0.282397	0.000065	1.467257	0.000077	0.001017	0.000024	0.0345961	0.0021851	-13.26157	1.3	646

	Total Hf (V)	176Hf/177Hf	2SE	Hf178/177	2 SE	Lu176/Hf177	2 SE	176Yb/177Hf	2 SE	εHf (t)	2 SE	Ref age
CMR07												
07Z1	11.78	0.28237	0.00008	1.46725	0.00008	0.0007	0.00004	0.025	0.00069	-14.35786	1.6	627.9
07Z2	12.75	0.28234	0.00007	1.46724	0.00009	0.00083	0.00002	0.02908	0.00117	-15.45415	1.38	650.8
07Z3	12.06	0.28229	0.00007	1.46735	0.00007	0.00065	0.00001	0.02451	0.00062	-17.01017	1.34	609.6
07Z4	12.83	0.28225	0.00007	1.46728	0.00009	0.0009	0.00002	0.0345	0.00156	-18.60156	1.46	648.1
07Z5	11.64	0.28239	0.00006	1.46723	0.0001	0.00109	0.00003	0.03171	0.00212	-13.40302	1.26	530
07Z7	11.61	0.28227	0.00007	1.46733	0.00008	0.00064	0.00001	0.02309	0.00062	-17.78818	1.46	650.3
07Z8	11.92	0.28238	0.00007	1.46725	0.00008	0.00061	0.00002	0.02196	0.00075	-13.89812	1.34	632.1
07Z9	10.55	0.28231	0.00007	1.46729	0.00009	0.00101	0.00004	0.03518	0.00132	-16.26752	1.44	638.8
07Z10	9.28	0.2824	0.00008	1.46726	0.00009	0.00225	0.00018	0.07156	0.00274	-13.15548	1.64	581.3
07Z11	12.47	0.28235	0.00007	1.46724	0.00008	0.00098	0.00002	0.029	0.00159	-15.10051	1.4	609.4
07Z12	12.14	0.28229	0.00007	1.46727	0.00009	0.00068	0.00001	0.02466	0.00072	-16.93944	1.36	628.4
07Z13	11.62	0.28238	0.00006	1.46724	0.00008	0.00088	0.0001	0.02451	0.00128	-14.03958	1.22	647.3
07Z14	13.16	0.28228	0.00008	1.46727	0.00009	0.00051	0.00001	0.01851	0.0004	-17.39918	1.62	659.3
07Z15	15.41	0.28226	0.00008	1.46735	0.00009	0.00085	0.00002	0.02874	0.00043	-18.0711	1.54	642.5
07Z16	14.87	0.28228	0.00009	1.46732	0.00011	0.00084	0.00002	0.02998	0.00077	-17.54063	1.8	657
07Z17	10.58	0.28228	0.00008	1.46731	0.0001	0.00067	0.00001	0.02606	0.00114	-17.39918	1.64	647.5
07Z18	11.12	0.28234	0.00007	1.46717	0.00007	0.0012	0.00006	0.03974	0.00222	-15.13587	1.48	628.3
07Z19	13.6	0.28225	0.00006	1.4673	0.00007	0.00061	0.00001	0.02276	0.00069	-18.35401	1.14	653.6
07Z20	12.58	0.28228	0.00007	1.46732	0.00007	0.00017	0	0.00612	0.00013	-17.29308	1.46	648.8
07Z21	9.612	0.28225	0.00008	1.46723	0.00008	0.00003	0	0.00159	0.00003	-18.60156	1.56	631.2
07Z22	10.45	0.2823	0.00006	1.46729	0.0001	0.00007	0	0.0027	0.00006	-16.69189	1.24	642.7
07Z23	13.85	0.28237	0.0001	1.46728	0.0001	0.00057	0.00004	0.01814	0.00082	-14.35786	1.9	628.9
07Z24	10.95	0.28243	0.00007	1.46721	0.00009	0.00098	0.00001	0.02784	0.00342	-11.95309	1.34	618.6
07Z25	10.46	0.28231	0.00007	1.46726	0.00009	0.0009	0.00003	0.0227	0.00132	-16.37362	1.32	651.5
07Z26	15.2	0.28242	0.00006	1.46718	0.00008	0.0015	0.00003	0.04335	0.00371	-12.62501	1.22	640.5
07Z27	12.18	0.28234	0.00007	1.4672	0.00008	0.00083	0.00002	0.02745	0.00126	-15.24196	1.34	614
07Z28	8	0.28278	0.0003	1.46681	0.00029	0.00159	0.0001	0.06516	0.02039	0.28291	6	663.9
07Z29	13.55	0.2823	0.00006	1.46733	0.00009	0.00084	0.00001	0.02866	0.00124	-16.72726	1.2	628.8
07Z30	9.09	0.28246	0.00009	1.4672	0.00011	0.00132	0.00005	0.04084	0.00406	-11.21045	1.88	625.7
CMR08												
08Z1	13.17	0.282289	0.000064	1.467245	0.000076	0.000705	0.000021	0.0220108	0.0010344	-17.081	1.28	627
08Z2	11.09	0.282265	0.000078	1.46738	0.00011	0.000853	0.000004	0.034574	0.0006684	-17.93	1.56	621.3
08Z3	12.63	0.282271	0.000078	1.467305	0.000083	0.001035	0.00002	0.0430086	0.0011342	-17.717	1.56	643
08Z4	12.82	0.282352	0.000054	1.467253	0.000068	0.000856	0.000041	0.0308532	0.0015632	-14.853	1.08	624.4
08Z5	12.07	0.282237	0.000083	1.467317	0.000093	0.000826	0.000015	0.0311983	0.0010585	-18.92	1.66	650.4
08Z6	12.17	0.282351	0.000067	1.467233	0.000096	0.000768	0.000019	0.0304188	0.0017037	-14.888	1.34	643
08Z7	12.16	0.282301	0.00006	1.467239	0.000083	0.000864	0.000022	0.0297597	0.0013589	-16.657	1.2	635.2
08Z8	13.27	0.282427	0.00007	1.467125	0.000098	0.001033	0.000013	0.0345286	0.0037993	-12.201	1.4	641
08Z9	9.35	0.282377	0.000074	1.467272	0.000094	0.001007	0.000023	0.0295957	0.002355	-13.969	1.48	668
08Z10	14.09	0.2823	0.000069	1.467296	0.000084	0.001186	0.000011	0.0434917	0.0016205	-16.692	1.38	633
08Z11	11.24	0.282333	0.000084	1.467264	0.000093	0.000839	0.000006	0.0312417	0.0016174	-15.525	1.68	654.6
08Z12	11.62	0.282422	0.000069	1.467186	0.000078	0.000872	0.000037	0.023462	0.0019352	-12.377	1.38	650.6
08Z13	9.88	0.282464	0.000077	1.46714	0.000097	0.000909	0.000042	0.0279269	0.0028176	-10.892	1.54	631.4
08Z14	13.53	0.282292	0.00006	1.46725	0.000062	0.001025	0.000018	0.0354602	0.0008297	-16.975	1.2	641.5
08Z15	9.54	0.28258	0.00011	1.46701	0.00012	0.001497	0.000064	0.0461735	0.0061304	-6.7899	2.2	654
08Z16	13.06	0.282332	0.000062	1.467254	0.000072	0.001268	0.000025	0.0367441	0.0018134	-15.56	1.24	615.7
08Z17	9.79	0.282368	0.000077	1.467284	0.000086	0.000961	0.000026	0.0298213	0.0013196	-14.287	1.54	632.9
08Z18	11.31	0.282339	0.000078	1.46723	0.00011	0.000937	0.000048	0.0354878	0.0015023	-15.313	1.56	639.4
08Z19	11.65	0.282369	0.000068	1.467214	0.000073	0.000879	0.000049	0.0253937	0.0012573	-14.252	1.36	630
08Z20	8.53	0.2825	0.000072	1.467063	0.000097	0.001119	0.000059	0.0304388	0.0040918	-9.6191	1.44	620
08Z21	11.52	0.282401	0.000067	1.46714	0.000065	0.000952	0.000022	0.0258624	0.002537	-13.12	1.34	642
08Z22	8.59	0.28235	0.000083	1.46723	0.0001	0.001481	0.000034	0.0472878	0.003186	-14.924	1.66	715
08Z23	12.13	0.28236	0.00014	1.46718	0.00016	0.000593	0.000051	0.0206786	0.0011171	-14.57	2.8	614
08Z24	12.82	0.282307	0.000066	1.467274	0.000079	0.000567	0.00001	0.0225546	0.0011394	-16.444	1.32	627
08Z25	11.487	0.282244	0.000064	1.467327	0.000082	0.00052	0.000032	0.0225293	0.0016854	-18.672	1.28	622
08Z26	7.46	0.282432	0.000073	1.46718	0.0001	0.000979	0.000035	0.0296211	0.0024528	-12.024	1.46	636
08Z27	9.55	0.282543	0.000062	1.467057	0.00008	0.001117	0.000084	0.0272608	0.0029658	-8.0984	1.24	667
08Z28	11.35	0.282468	0.000087	1.467155	0.000092	0.0012	0.000061	0.0385814	0.002361	-10.751	1.74	589.3

5. Discussion and Conclusion

5.1. Petrogenesis, Evolution and Significance of Granitoid Intrusions in the Bétaré Oya Gold District

Zircon external and internal structures have been used to distinguish pristine magmatic zircons and resorbed zircons derived from residual melts through mixing [40]. These categories of zircon populations exist in the granitoid investigated. The pristine magmatic zircons are generally euhedral displaying oscillatory and /or sector zoning whereas the resorbed zircons are characterized by corroded and resorption surfaces, recrystallized quartz and mineral inclusions. U vs Y and Y vs Yb/Sm discriminant plots (Figure 6a and Figure 6b) show that the Bétaré Oya granitic pluton varies from granodiorite to tonalite. Their

REE normalized patterns dominantly show high Ce concentrations, negative Eu anomaly and enrichment in HREE which are characteristics of crustal derived magmas [41]. However, some of the zircons from sample CMR08 display REE patterns with positive Eu anomalies and we attribute this to zircon formation at different stages of magma evolution. Eu exists as a divalent (Eu^{2+}) and a trivalent (Eu^{3+}) cation. The Eu^{2+} readily substitutes for Ca^{2+} in plagioclase in a reducing environment fractionating Eu from the melt hence resulting in a negative Eu anomaly whereas Eu^{3+} is incompatible and will remain in the magma resulting to a positive Eu anomaly. The negative Eu anomaly exhibited by most grains Eu fractionation into plagioclase whereas the positive Eu anomaly depicts the influx of magma void of plagioclase. This therefore further suggests the phenomenon of magma mixing during the magma evolution. According to [42] the positive Eu anomaly suggests that the zircons crystallized from a highly evolved melt where most of the plagioclase was already fractionated. The Ce/Sm ratio is used as a representation of oxidation conditions while Yb/Gd ratio evaluates the evolution of magma by fractional crystallization. The Ce/Sm ratios range of 0 to 3 associated with variable Yb/Gd ratios upto 76 in zircons from the Bétaré Oya granitoid are characteristic features of crustal derived melt in a reducing environment. Th/U ratios between 0.1 and 1 with most values falling below 1.0 as well as a negative correlation observed between Th/U and Hf concentration and an almost constant Th concentration with increase in U/Ce ratio all confirm that the granitoids are derived from crustal recycling. The emplacement temperatures of this granitoid range from 625°C to 775°C and this is consistent with temperatures for S-type granitoids based on the classification of [43]. Such temperatures however have been reported in the northern parts of the CASZ by [18] for I-type granitoid of high K-calc alkaline composition using hornblende in plagioclase with temperature values of 698 and 720 °C for the Djourde granitoids, 698 - 728 °C for the Sinassi granitoids and 667- 670°C for the orthogneiss. Zircon morphology (the existence of dark rounded cores with magmatic overgrowths is clear evidence of inherited zircons) and chemistry coupled with the tectonic setting of the study area (a pull a part basin) provide evidence of metasedimentary contribution during magma generation. Hf as a minor element in zircon is a very sensitive tracer of crustal and mantle processes [44] hence its concentration is vital in unveiling the petrogenesis of the Bétaré-Oya granitic pluton. All three samples from this intrusion are characterized by high Hf concentration (>10000 ppm, Table 3). According to [45], residual and depleted mantle are characterized by Lu/Hf ratio > chondrite values and will be radiogenic with positive ε_{Hf} value. In contrast to this, enriched ancient crust tends to have Lu/Hf ratios < chondrite values and is unradiogenic with negative ε_{Hf}. $^{176}Lu/^{177}Hf$ ratio for the Bétaré Oya granitic samples are generally less than chondrite values (0.022) and along with negative ε_{Hf} values are evidence of a crustal source whereas the few positive values just above CHUR and below the Depleted Mantle (DM1) line points to a mafic crust contribution (Figure 9).

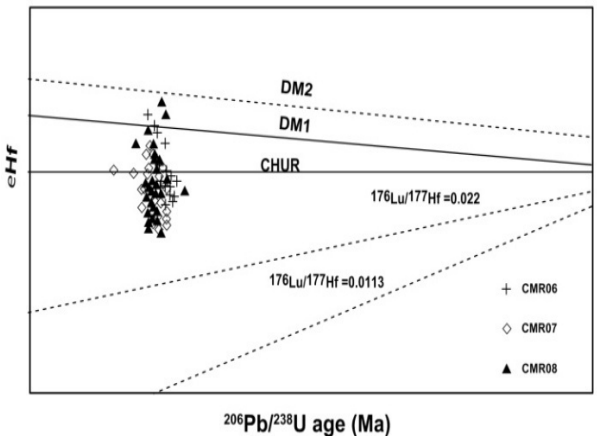

Figure 9. Epsilon Hf versus $^{206}Pb/^{238}U$ ages diagram showing the studied samples together with crustal evolution trends of average crust ($^{176}Lu/^{177}Hf$ = 0.0113), mafic crust ($^{176}Lu/^{177}Hf$ = 0.022), and Depleted mantle evolution trends DM1 and DM2 [48]

Geochronological studies along the Central Cameroon Shear Zone (CCSZ) have reported various Pan African ages for granitic intrusions [13]. These ages vary from 626 to 654 Ma for leusosomes of the Yaoundé series [17], 603 - 618Ma for the Mayo Punko metadiorite and 560 - 611Ma for the Mayo IIou metagranodiorite [46] in the northern region of Cameroon. Recently, [18] dated the Sinassi batholith at 644 - 686 Ma while in the western domain, [15] dated the Fomopéa complex at 610Ma, the Ngondo plutonic complex at 602Ma [47]. The Ekomédion two mica granite reveal an age of 578 Ma [16,18]. Ages of the Batouri granitoid lie within the 640 - 620 Ma age bracket [7]. A mean age of 635 Ma was obtained for granitic pluton within the Bétaré-Oya Gold District. This age is attributed to the emplacement age of the pluton and falls within the age bracket obtained by [7]. The age range defines an extensive unique Pan African melting event contemporaneous with the magmatism and deformation (sinistral shear movement) responsible for the emplacement of granitic plutons along the CCSZ.

Mineralization along the CCSZ and the Patos/Pernamboco shear zones in NE Brazil are known to be associated with late granitoid intrusions. In NE Brazil mineralization is known to be associated with younger granitic plutons generally 570 - 580Ma. This age bracket is known for its tungsten, gold (skarn and quartz vein type) uranium and molybdonium deposits. This mineralization age is well represented in Cameroon by the U-Mo mineralization in Ekomédion. This study reveals a new and older mineralization along the CCSZ at 620 - 635Ma for the Bétaré Oya Gold District, SE Cameroon. This mineralization is seemingly absent across the Atlantic. We therefore suggest that exploration effort in the region should revisit older granitoids for Au, W, Mo, U mineralization amongst others.

5.2. Conclusion

1) Whole rock chemistry defines the Bétaré Oya granitoid as high K Calc-alkaline to sub-alkaline in nature. It is granodioritic to tonalitic in composition, peraluminous and of I-type emplaced within a volcanic arc

setting at a temperature that varies between 625°C and 775°C

2) Internal structures such as zoning, resorption zone, corrosive surfaces and mineral inclusions were used in this study to distinguish between magmatic and metamorphic zircons. The co-existence of zircon grains with clear oscillatory zoning (characteristic of igneous zircon) associated with zircon grains showing corroded crystal outlines and resorption surfaces suggest recrystallization of zircon grains as a result of hot magma influx.

3) REE discriminant patterns clearly shows positive Ce concentrations, negative Eu anomaly and HREE enrichment coupled with Lu/Hf ratios <0.022 and negative ε_{Hf} values points to a crustal source of magma with mafic crust contribution.

4) U-Pb age by LA ICP MS revealed that granitic intrusions within the Bétaré Oya Gold District are Pan African in age with a mean age of 635 Ma similar to previously obtained ages along the CCSZ and defines a unique melting event synchronous with magmatism and deformation for the emplacement of granitoids along this structure. The mean age of the granodiorite intrusion in the Oya Gold District at 635 Ma defines a new and older mineralization age along the Braziliano-Pan African region

Acknowledgements

This publication is part of the PhD thesis of the first author underway in the University of Buea. Prof. John Cottle of the Department of Earth Sciences & Earth Research Institute of the University of California assisted with the geochronological analyses. Prof. Bernd Lehmann is greatly thanked for helping with the isochron plots. Special thanks go to Ashu Jones Egbe for helping with the geologic maps used in this publication.

References

[1] Pirajno, F., Hydrothermal processes and mineral systems. Springers science Business Media B.V, Dordrecht, 2009.

[2] Gagnevin, D., Daly, J.S., Kronz, A., Zircon texture and chemical composition as a guide to magmatic processes and mixing in a granitic environment and coeval volcanic system. Contribution to Mineral Petrology 159, 579-596, 2010.

[3] Belousova, E.A., Griffin W.L., O'reilly S.Y., Fisher N.I., Igneous zircon: trace element composition as an indicator of source rock type. Contribution to Mineral Petrology 143, 602-622, 2002.

[4] Erdmann, S., Wodicka, N., Jackson, S.E., Corrigan, D., Zircon textures and composition: refractory recorders of magmatic volatile evolution? Contribution to Mineral Petrology 165, 45-71, 2013.

[5] Matteini, M., Dantas, E.L., Pimentel, M.M., Bühn, B., Combined U-Pb and Lu-Hf isotope analyses by laser ablation MC-ICP-MS: methodology and applications. Anais da Academia Brasileira de Ciências, 82, 479-491, 2010.

[6] Suh, C.E., Lehmann, B., Mafany, G.T., Geology and geochemical aspects of lode gold mineralization at Dimako-Mboscorro, SE Cameroon. Geochemistry: Exploration, Environment, Analysis, 6, 295-309, 2006.

[7] Asaah, A.V., Zoheir B., Lehmann B., Burgess D.F.R., Suh E.C., Geochemistry and geochronology of the ~620 Ma gold-associated Batouri granitoids, Cameroon. International Geology Review, 2014.

[8] Vishiti, A., Suh, C.E., Lehmann, B., Egbe, J.A., Shemang, E.M., Gold grade variation and particle microchemistry in exploration pits of the Batouri gold district, SE Cameroon. Journal of African Earth Sciences 111, 1-13, 2015.

[9] Njongfang, E., Ngako, V., Moreau, C., Affaton, P., Diot, H., Restraining bends in high temperature shear zones: the "Central Cameroon Shear Zone", Central Africa. Journal of African Earth Sciences, 52, 9-20, 2008.

[10] Toteu, S.F., Van Schmus, W.R., Penaye, J., Michard, A., New U-Pb and Sm-Nd data from north central Cameroon and its bearing on the Pre-Pan-African his-tory of Central Africa. Precambrian Research, 108, 45-73, 2001.

[11] Neves, S.P., Brugueir, O., Vauchez, A., Bosch, D., Silva, J.M.R., Mariano, G., Timing of crust formation, deposition of supracrustal sequences, and Transamazonian and Brasiliano metamorphism in the East Pernambuco belt (Borborema Province, NE Brazil): Implications for western Gondwana assembly. Precambrian Research, 149, 197-216, 2006.

[12] Van Schmus, W.R., Oliveira, E.P., Da Silva Filho, A.F., Toteu, S.F., Penaye, J., Guimarães, I.P., The Central African Fold Belt Proterozoic Links between the Borborema Province, NE Brazil, and the Central African Fold Belt. Geological Society, London, Special Publications 294, 69-99, 2008.

[13] Penaye, J., Krõner, A., Toteu, S.F., Van Schmus, W.R., Doumnang, J.C., Evolution of the Mayo Kebbi region as revealed by zircon dating: an early (ca.740 Ma) Pan-African magmatic arc in southwestern Chad. Journal of African Earth Science 44, 530-542, 2006.

[14] Bouyo, H.M., Toteu, S.F., Deloule, E., Penaye, J., Van Schmus, W.R., U-Pb and Sm-Nd dating of high-pressure granulites from Tcholliré and Banyo regions: evidence for a Pan-African granulite facies metamorphism in north-central Cameroon. Journal of African Earth Science, 54, 144-154, 2009.

[15] Kwekam, M., Liégeois, J.P., Njonfang, E., Affaton, P., Hartmann, G., Tchoua, F., Nature, origin and significance of the Pan-African high-K calc-alkaline Fomopea plutonic complex in the Central African fold belt (Cameroon). Journal of African Earth Science 57, 79-95, 2010.

[16] Mosoh Bambi,.C.K., Frimmel, H.E., Zeh, A., Suh, C.E., Age and origin of Pan-African granites and associated U-Mo mineralization at Ekomédion, southwestern Cameroon. Journal of African Earth Sciences 88, 15-37, 2013.

[17] Ngnotue, T., Ganno, S., Nzenti, J.P., Schulz, B., Tchaptchet, T.D., Suh, C.E., Geochemistry and Geochronology of Peraluminous High-K Granitic Leucosomes of Yaoundé Series (Cameroon): Evidence for a unique Pan-African Magmatism and Melting Event in North Equatorial Fold Belt. International Journal of Geosciences, 3, 525-548, 2012.

[18] Bouyo, H.M., Penaye, J., Njel, U.O., Moussango, A.P.I., Sep J.P.N., Nyama, B. A., Wassouo, W.J.J., Abaté, M.E., Yaya, F., Mahamat, A., Hao, Ye, Fei Wu, Geochronological, geochemical and mineralogical constraints of emplacement depth of TTG suite from the Sinassi Batholith in the Central African Fold Belt (CAFB) of northern Cameroon: Implications for tectonomagmatic evolution. Journal of African Earth Sciences 116, 9-41, 2016.

[19] Ngako, V., Affaton, P., Nnange, J.M., And Njanko, T.H., Pan-African tectonic evolution in central and southern Cameroon: Transpression and transtension during sinistral shear movements; Journal of African Earth Science 36, 207-214, 2003.

[20] Kankeu, B., Greiling, R.O., Nzenti, J.P., Bassahak, J., Hell, V.J., Strain partitioning along the Neoproterozoic central Africa shear zone system: Structures and magnetic fabrics (AMS) from the Meiganga area, Cameroon;Neues Jahrbuch für Paläontologie - Abhand-lungen 265,27-47, 2012.

[21] Dane, A., "Lom River Property: Geological Report," Bridge Consulting, 86, 1998.

[22] Soba, D., "La Série de Lom: Étude Géologique et Géochronologique du Bassin Vocano-Sédimentaire de la Chaine Panafricaîne à l'Est du Cameroun," Thèse de doctoral d'Etat, Université Pierre et Marie Curie, Paris, 1989.

[23] Kylander-Clark, R.C.A., Bradley, R., Hacker, Cottle, J.M., Laser-ablation split-stream ICP petrochronology. Chemical Geology 345, 99-112, 2013.

[24] Mckinney, S.T., Cottle, J.M., And Lederer, G.W., Evaluating rare earth element (REE) mineralization mechanisms in Proterozoic gneiss. Music valley,California, Geological Society of America Bulletin, B31165, 1, 2015.

[25] Paton, C., Woodhead, J.D., Hellstrom, J.C., Hergt, J.M., Greig, A. And Maas, R., Improve laser ablation U-Pb zircon geochronology through roburst downhole fractionation correction. Geochemistry Geophysics geosystems 11, 1525-2027, 2010.

[26] Wiedenbeck, M., Allé, P., Corfu, F., Griffin, W.L., Meier, M., Oberli, F., Von Quadt, A., Roddick, J.C., Spiegel, W., Three natural zircon standards for U-Th-Pb, Lu-Hf, trace element and REE analyses. Geostandard Newsletters, 19, 1-23, 1995.

[27] Horstwood, M., Kosler, J., Gehrels G., Jackson, S.,E., McLean N.,M., Paton, C., Pearson, N.,J., Sircombe, K., Sylvester, P., Vermeesch, P., Bowring, J., F., Condon, D.,J., Schoene, B., Community derived standards for LA-ICP-MS U-Th-Pb Geochronology - Uncertainty propagation, Age interpretation and reporting; Geostandards and Geoanalytical research, 40, 311-332, 2016.

[28] Liu, Y., Hu, Z., Zong, K., Gao, C., Gao, S., Xu, J., Chen, H., Reappraisement and refinement of zircon U-Pb isotope and trace element analyses by LA-ICP-MS. Chinese Science Bulletin, 55, 1535-1546, 2010.

[29] Bowring, J.F., Mclean, N.M., Bowring, S.A., Engineering cyber infrastructure for U-Pb geochronology: Tripoli and U-Pb Redux. Geochemistry Geophysics Geosystems 12: 2011.

[30] Hagen-Peter, G., Cottle, J.M., Tulloch, J.A., Cox, S.C., Mixing between enriched lithospheric mantle and crustal components in a short-lived subduction-related magma system, Dry Valleys area, Antarctica: Insights from U-Pb geochronology, Hf isotopes, and whole-rock geochemistry. Lithosphere 7 (2), 174-188, 2015.

[31] Scherer, E., Münker, C., Mezger, K., Calibration of the lutetium-hafnium clock. Science 293, 683-686, 2001.

[32] Söderlund, U., Patchett, P.J., Vervoort, J.D., Isachsen, C.E., The 176Lu decay constant determined by Lu-Hf and U-Pb isotope systematics of Precambrian mafic intrusions. Earth Planetary Science Letter, 219, 311-324, 2004.

[33] Bouvier, A., Vervoort, J.D., Patchett P.J.,The Lu-Hf and Sm-Nd isotopic composition of CHUR: constraints from unequilibrated chondrites and implications for the bulk composition of terrestrial planets. Earth Planetary Science Letter, 273, 48-57, 2008.

[34] Ferry, J. M., Watson, E. B., New thermodynamic models and revised calibrations for the Ti-in-zircon and Zr-in-rutile thermometers. *Contributions to Mineralogy & Petrology*, 154, 429-437, 2007.

[35] MacDonald, G.A., and Katsura, T., Chemical composition of Hawaiian lavas1: Journal of Petrology, 5, 82-133, 1964.

[36] Rickwood, P.C., Boundary lines within petrologic diagrams which use oxides of major and minor elements: Lithosphere, 22, 247-263, 1989.

[37] Peccerillo, A., and Taylor, S.R., Geochemistry of Eocene calc-alkaline volcanic rocks from the Kastamonu area, Northern Turkey: Contributions to Mineralogy and Petrology, 58, 63-81, 1976.

[38] Maniar, P.D., and Piccoli, P.M., Tectonic discrimination of granitoids: Geological Society of America Bulletin, 101, 635-643, 1989.

[39] Pearce, J.A., Harris, N.B.W., and Tindle, A.G., Trace element discrimination diagrams for the tectonic interpretation of granitic rocks: Journal of Petrology, 25, 956-983, 1984.

[40] Yuanbao, W., U. and Yongfei, Z., Genesis of zircon and its constraints on interpretation of U-Pb age Chinese Science Bulletin, 49, 1554-1569, 2004.

[41] Muňoz, M., Charrier, R., Fanning, C.M., Maksaev, V., Deckart, K., ZirconTrace Element and O-Hf IsotopeAnalyses of Mineralized Intrusions from El Teniente Ore Deposit, Chilean Andes: Constraints on the Source and Magmatic Evolution of Porphyry Cu-Mo Related Magmas. Journal of Petrology 1-32, 2012.

[42] Castiñeiras, P., Navidad, M., Casas, J.M., Liesa, M., Carreras, J., Petrogenesis of Ordovician Magmatism in the Pyrenees (Albera and Canigó Massifs) Determined on the Basis of Zircon Minor and Trace Element Composition. Journal of Geology, 119, 521-534, 2011.

[43] Chappell, B.W., and White, A.J.R., Two contrasting granite types Pacific Geology 8, 173-174, 1974.

[44] Belousova, E.A., Griffin, W.L., O'reill, Y.S., Zircon Crystal Morphology, Trace Element Signatures and Hf Isotope Composition as a Tool for Petrogenetic Modelling: Examples from Eastern Australian Granitoids. Journal of Petrology, 47, 329-353, 2006.

[45] Ji, W.Q., Wu F.Y., Chung, S.L., Li J.X., Liu, C.Z., Zircon U-Pb geochronological and Hf isotopic constraints on petrogenesis of the Ganddese batholith, southern Tibet. Chemical Geology, 262, 229-245, 2009.

[46] Toteu, S.F., Michard, A., Bertrand, J.M., Rocci, G., U-Pb dating of Precambrian rocks from northern Cameroon, orogenic evolution and chronology of the Pan-African belt of central Africa. Precambrian Research, 37, 71-87, 1987.

[47] Tagne-Kamga, G., Petrogenesis of the Neoproterozoic Ngondo Plutonic complex (Cameroon, west central Africa): a case of late-collisional ferropotassic magmatism. Journal of African Earth Science, 36, 149-171, 2003.

[48] Maibam, B., Gerdes, A., Goswami, J., N., U-Pb and Hf isotope records in detrital and magmatic zircon from eastern and western Dharwar craton, southern India: Evidence for coeval Archaean crustal evolution. Precambian Research, 275, 496-512, 2016.